LUND UNIVERSITY

Optimization of breast tomosynthesis: Computer simulations of image acquisition and glandular dose

Förnvik, Hannie

2018

Document Version:
Publisher's PDF, also known as Version of record

Optimization of breast tomosynthesis

Computer simulations of image acquisition and glandular dose

HANNIE FÖRNVIK
MEDICAL RADIATION PHYSICS, MALMÖ | FACULTY OF MEDICINE | LUND UNIVERSITY

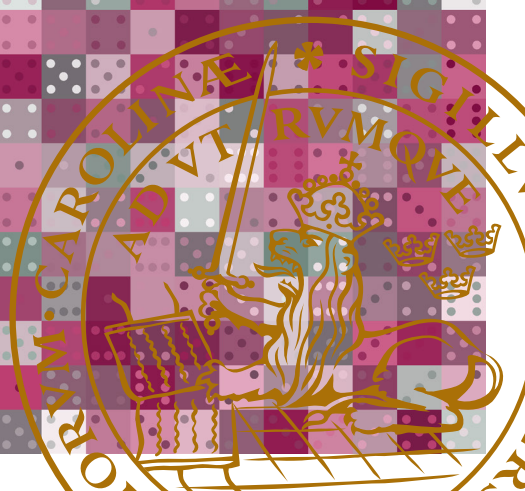

Optimization of breast tomosynthesis

Computer simulations of image acquisition and glandular dose

Hannie Förnvik

LUND
UNIVERSITY

DOCTORAL DISSERTATION
by due permission of the Faculty of Medicine, Lund University, Sweden.
To be defended at Clinical Research Center, room 93-09-002, Jan Waldenströms gata 35, Malmö, June 5, 2018 at 9:00.

Faculty opponent
Susan Astley, PhD, Division of Informatics, Imaging and Data Sciences, Faculty of Biology, Medicine and Health, University of Manchester, UK

Organization LUND UNIVERSITY	Document name DOCTORAL DISSERTATION
Medical Radiation Physics, Malmö Department of Translational Medicine Skåne University Hospital 205 02 Malmö	Date of issue June 5, 2018
Author(s) Hannie Förnvik	Sponsoring organization

Title and subtitle

Optimization of breast tomosynthesis: Computer simulations of image acquisition and glandular dose

Abstract

Breast tomosynthesis (BT) is an X-ray imaging technique recently introduced as an alternative or complement to standard digital mammography (DM) in breast imaging and breast cancer screening. In BT, a set of projection images is acquired over a limited angular range and reconstructed into a volume of slice images. The method includes many possible combinations of acquisition parameters that have to be optimized for best possible clinical performance and outcome. The visibility of breast cancer lesions is important in this context. Compared to DM images, the reconstructed BT volume provides additional information on depth, reducing the superposition of breast tissue, which may hide true lesions or appear as false positive findings. Thus, the BT volume also contains information about the distribution of dense tissue within the breast, which is of interest when estimating the radiation dose from DM and BT exposure.

In this thesis, a simulation procedure was developed for the optimization of image acquisition and estimation of individual glandular dose in BT. The procedure was shown to be useful in generating BT images with realistic sharpness, though with higher image noise and contrast than experimentally acquired images (Paper I). The procedure was used to investigate the influence of angular range, distribution of projection images, and dose distribution on simulated microcalcifications in reconstructed BT volumes. Image acquisitions with very high central dose yielded significantly lower visibility than acquisitions with more uniform dose distributions, and the depth resolution increased with wider angular range (Paper II).

A method for localizing dense tissue from reconstructed BT volumes was verified using the simulation procedure (Paper III). A prototype software program was used for automatic and objective estimation of breast density in BT, with similar performance as DM (Paper IV). Using software breast phantoms recreated from reconstructed BT volumes, the glandular dose could be estimated with good overall accuracy for breast phantoms with different amounts and distributions of dense tissue (Paper V).

The developed simulation procedure has been a useful tool for optimizing acquisition parameters and estimating glandular dose in BT. The procedure could potentially be developed for further evaluation of the imaging chain and estimation of individual glandular dose in human cases.

Key words

breast tomosynthesis, Monte Carlo simulation, acquisition parameters, software breast phantom, microcalcifications, breast density, glandular dose, glandular distribution

Classification system and/or index terms (if any)

Supplementary bibliographical information		Language English
ISSN and key title 1652-8220		ISBN 978-91-7619-637-3
Recipient's notes	Number of pages	Price
	Security classification	

Signature Date April 18, 2018

Optimization of breast tomosynthesis

Computer simulations of image acquisition and glandular dose

Hannie Förnvik

LUND
UNIVERSITY

Front cover: Illustration by Hannie Förnvik.

Back cover: Word cloud generated at Wordclouds.com.

Medical Radiation Physics, Malmö
Department of Translational Medicine
Faculty of Medicine

ISBN 978-91-7619-637-3
ISSN 1652-8220

Printed in Sweden by Media-Tryck, Lund University
Lund 2018

MADE IN SWEDEN

Inför Gud är vi alla smålänningar.

Gammalt talesätt

Contents

Abbreviations

2D	Two-dimensional
3D	Three-dimensional
AEC	Automatic exposure control
ASFW	Artefact spread function width
BI-RADS	Breast Imaging-Reporting and Data System
BT	Breast tomosynthesis
CC	Craniocaudal
CDF	Contrast degradation factor
CT	Computed tomography
DM	Digital mammography
FBP	Filtered back-projection
LM	Lateromedial
MGD	Mean glandular dose
MLO	Mediolateral oblique
MRI	Magnetic resonance imaging
NNPS	Normalized noise power spectrum
PET	Polyethylene terephthalate
PMMA	Polymethyl methacrylate
ROI	Region of interest
SDNR	Signal-difference-to-noise ratio
SRSAR	Super-resolution reconstruction with statistical artefact reduction
VBD	Volumetric breast density

Abstract

Breast tomosynthesis (BT) is an X-ray imaging technique recently introduced as an alternative or complement to standard digital mammography (DM) in breast imaging and breast cancer screening. In BT, a set of projection images is acquired over a limited angular range and reconstructed into a volume of slice images. The method includes many possible combinations of acquisition parameters that have to be optimized for best possible clinical performance and outcome. The visibility of breast cancer lesions is important in this context. Compared to DM images, the reconstructed BT volume provides additional information on depth, reducing the superposition of breast tissue, which may hide true lesions or appear as false positive findings. Thus, the BT volume also contains information about the distribution of dense tissue within the breast, which is of interest when estimating the radiation dose from DM and BT exposure.

In this thesis, a simulation procedure was developed for the optimization of image acquisition and estimation of individual glandular dose in BT. The procedure was shown to be useful in generating BT images with realistic sharpness, though with higher image noise and contrast than experimentally acquired images (**Paper I**). The procedure was used to investigate the influence of angular range, distribution of projection images, and dose distribution on simulated microcalcifications in reconstructed BT volumes. Image acquisitions with very high central dose yielded significantly lower visibility than acquisitions with more uniform dose distributions, and the depth resolution increased with wider angular range (**Paper II**).

A method for localizing dense tissue from reconstructed BT volumes was verified using the simulation procedure (**Paper III**). A prototype software program was used for automatic and objective estimation of breast density in BT, with similar performance as DM (**Paper IV**). Using software breast phantoms recreated from reconstructed BT volumes, the glandular dose could be estimated with good overall accuracy for breast phantoms with different amounts and distributions of dense tissue (**Paper V**).

The developed simulation procedure has been a useful tool for optimizing acquisition parameters and estimating glandular dose in BT. The procedure could potentially be developed for further evaluation of the imaging chain and estimation of individual glandular dose in human cases.

Populärvetenskaplig sammanfattning (Summary in Swedish)

Bröstcancer är den vanligaste typen av cancer bland kvinnor och fler än 8000 fall diagnostiseras varje år i Sverige. För att få en god prognos är det viktigt att upptäcka cancern i ett tidigt stadium så att man kan ställa diagnos och påbörja behandling. Därför erbjuds alla kvinnor mellan 40 och 74 år regelbundna hälsoundersökningar (screening) med mammografi. Vid mammografi används röntgenstrålning med låg energi för att ta detaljrika tvådimensionella bilder av bröstet.

Alla cancrar upptäcks inte med mammografi, till stor del på grund av överlagringen av bröstvävnad i bilden vilket kan gömma misstänkta förändringar. Man kan också undersöka bröstet med hjälp av ultraljud, datortomografi (CT) eller magnetisk resonanstomografi (MR), men ingen av dessa bildtekniker har kunnat ersätta mammografi i bröstcancerscreening. En metod som däremot kan komma att komplettera eller ersätta mammografi i framtida screening är brösttomosyntes, en 3D-tekink som nyligen introducerades som ett alternativ för bildtagning av bröst. Undersökning med brösttomosyntes sker på liknande sätt som med mammografi med skillnaden att röntgenröret roterar en begränsad vinkel över bröstet medan en uppsättning röntgenbilder tas. Dessa bilder används sedan för att skapa en volym av snittbilder. Metoden innebär att det finns flera möjliga kombinationer av insamlingsparametrar som vinkelomfång, antal bilder och dosfördelning. För att uppnå bästa kliniska resultat måste bildinsamlingen optimeras utifrån hur dessa parametrar påverkar bildkvaliteten och synligheten av förändringar.

Genom att få tvärsnittsbilder av bröstet kan brösttomosyntes separera strukturer som vid avbildning med mammografi hade överlagrats i mammografibilden. Detta gör det lättare att urskilja små tumörer och mikroförkalkningar, vilka kan vara tidiga tecken på bröstcancer. Bildvolymen innehåller också information om fördelningen av tät bröstvävnad i bröstet, vilket är av intresse vid uppskattning av stråldos från mammografi- och brösttomosyntesundersökningar.

I det här avhandlingsarbetet utvecklades en rutin för datorsimulering av bildinsamling och uppskattning av stråldos i brösttomosyntes. Metoden visades vara användbar för att simulera brösttomosyntesbilder med liknande skärpa, men med något högre brus och kontrast jämfört med bilder tagna med maskinen (**arbete I**).

Simuleringsrutinen användes för att undersöka bildinsamlingar med olika vinkelomfång, bildfördelningar och dosfördelningar. Insamling med hög central dosfördelning medförde sämre synlighet av simulerade mikroförkalkningar än insamling med mer jämna dosfördelningar, medan ett bredare vinkelomfång ökade upplösningen i djupled (**arbete II**).

En metod för att lokalisera tät bröstvävnad i rekonstruerade bildvolymer verifierades med hjälp av simuleringsmetoden (**arbete III**). Nyutvecklad programvara användes för att på ett automatiskt och objektivs sätt uppskatta brösttäthet i brösttomosyntes med liknande resultat som i mammografi (**arbete IV**). Utifrån bröstfantom baserade på rekonstruerade bildvolymer kunde stråldosen uppskattas för olika mängder och fördelningar av tät bröstvävnad (**arbete V**).

Den framtagna simuleringsrutinen är ett användbart verktyg för optimering av insamlingsparametrar och uppskattning av stråldos i brösttomosyntes. Metoden skulle kunna utvecklas för fortsatt utvärdering av bildinsamlingen och beräkning av individuell stråldos till människor.

List of papers

Original papers

This thesis is based on the following five papers, which will be referred to by their Roman numerals:

I. Validation of a simulation procedure for generating breast tomosynthesis projection images

HANNIE PETERSSON[1], Lucy M. Warren, Anders Tingberg, Magnus Dustler and Pontus Timberg. *Radiation Protection Dosimetry*, 169 (1-4), 386-391, doi: 10.1093/rpd/ncv555 (2016)

II. Monte Carlo simulation of breast tomosynthesis: visibility of microcalcifications at different acquisition schemes

HANNIE PETERSSON, Magnus Dustler, Anders Tingberg and Pontus Timberg. *Proceedings of SPIE 9412, Medical Imaging 2015: Physics of Medical Imaging*, 94121H, doi: 10.1117/12.2081942 (2015)

III. Volumetric localisation of dense breast tissue using breast tomosynthesis data

Magnus Dustler, HANNIE PETERSSON and Pontus Timberg. *Radiation Protection Dosimetry*, 169 (1-4), 392-397, doi: 10.1093/rpd/ncw022 (2016)

IV. Comparison between software volumetric breast density estimates in breast tomosynthesis and digital mammography images in a large public screening cohort

Daniel Förnvik, HANNIE FÖRNVIK, Andreas Fieselmann, Kristina Lång and Hanna Sartor. *Submitted to European Radiology, under revision* (2018)

[1] Hannie Petersson changed her name to Hannie Förnvik in September 2017.

V. Breast dosimetry simulation using software phantoms and volumetric localization of glandular breast tissue from reconstructed breast tomosynthesis volumes

HANNIE FÖRNVIK, Pontus Timberg, Magnus Dustler, Daniel Förnvik, Sophia Zackrisson and Anders Tingberg. *Submitted to Medical Physics, under revision* (2018)

Published papers have been reproduced with kind permission from Oxford University Press (**Paper I** and **Paper III**) and SPIE (**Paper II**).

Other publications by the author

- Application of the fractal Perlin noise algorithm for the generation of simulated breast tissue

  Magnus Dustler, Predrag Bakic, HANNIE PETERSSON, Pontus Timberg, Anders Tingberg and Sophia Zackrisson. *Proceedings of SPIE 9412, Medical Imaging 2015: Physics of Medical Imaging*, 94123E, doi: 10.1117/12.2081856 (2015)

- Detection of calcification clusters in digital breast tomosynthesis slices at different dose levels utilizing a SRSAR reconstruction and JAFROC

  Pontus Timberg, Magnus Dustler, HANNIE PETERSSON, Anders Tingberg and Sophia Zackrisson. *Proceedings of SPIE 9416, Medical Imaging 2015: Image Perception, Observer Performance, and Technology Assessment*, 941604, doi: 10.1117/12.2081879 (2015)

- Evaluation of the possibility to use thick slabs of reconstructed outer breast tomosynthesis slice images

  HANNIE PETERSSON, Magnus Dustler, Anders Tingberg and Pontus Timberg. *Proceedings of SPIE 9787, Medical Imaging 2016: Image Perception, Observer Performance, and Technology Assessment*, 97871M, doi: 10.1117/12.2216688 (2016)

- Beam quality correction factors for KAP meters for lightly and heavily filtered X-ray beams

  Lars Herrnsdorf and HANNIE PETERSSON. *Radiation Protection Dosimetry*, 169 (1-4), 347-352, doi: 10.1093/rpd/ncw042 (2016)

- The characteristics of malignant breast tumors imaged using a prototype mechanical imaging system as an adjunct to mammography

  Magnus Dustler, Daniel Förnvik, Pontus Timberg, HANNIE PETERSSON, Anders Tingberg and Sophia Zackrisson. *Breast Imaging, IWDM 2016, LNCS 9699*, 282-288, doi: 10.1007/978-3-319-41546-8_36 (2016)

- Breast density assessment using breast tomosynthesis images

  Pontus Timberg, Andreas Fieselmann, Magnus Dustler, HANNIE PETERSSON, Hanna Sartor, Kristina Lång, Daniel Förnvik and Sophia Zackrisson. *Breast Imaging, IWDM 2016, LNCS 9699*, 197-202, doi: 10.1007/978-3-319-41546-8_26 (2016)

- Can mechanical imaging increase the specificity of mammography screening?

  Magnus Dustler, Daniel Förnvik, Pontus Timberg, Ingvar Andersson, HANNIE PETERSSON, Håkan Brorson, Anders Tingberg and Sophia Zackrisson. *European Radiology*, 27 (8), 3217-3225, doi: 10.1007/s00330-016-4723-6 (2017)

- Towards determination of individual glandular dose

  HANNIE FÖRNVIK, Pontus Timberg, Magnus Dustler, Daniel Förnvik, Sophia Zackrisson and Anders Tingberg. *Proceedings of SPIE* 10573*, Medical Imaging 2018: Physics of Medical Imaging*, 1057304, doi: 10.1117/12.2293454 (2018)

Preliminary reports

- Validation of a simulation procedure for generating breast tomosynthesis projection images

  HANNIE PETERSSON, Lucy M. Warren, Anders Tingberg, Magnus Dustler and Pontus Timberg. *Optimisation in X-ray and Molecular Imaging*, Göteborg, Sweden, May 2015

- Research highlights in Malmö breast tomosynthesis group

  Pontus Timberg, Magnus Dustler and HANNIE PETERSSON. *Nordic Congress of Radiology – Röntgenveckan*, Malmö, Sweden, September 2015

- A strategy to reduce image reading time in breast tomosynthesis

  HANNIE PETERSSON, Magnus Dustler and Pontus Timberg. *Nationellt möte om sjukhusfysik*, Falkenberg, Sweden, November 2015

- Evaluation of the possibility to use thick slabs of reconstructed outer breast tomosynthesis slice images

  HANNIE PETERSSON, Magnus Dustler, Anders Tingberg and Pontus Timberg. *Malmö Cancer Center Retreat*, Båstad, Sweden, September 2016

- Breast dosimetry simulation using volumetric localization of dense breast tissue from breast tomosynthesis data: current status

  HANNIE PETERSSON, Pontus Timberg, Daniel Förnvik, Anders Tingberg and Magnus Dustler. *Nationellt möte om sjukhusfysik*, Kolmården, Sweden, November 2016

- Towards determination of individual glandular dose

  HANNIE FÖRNVIK, Magnus Dustler, Daniel Förnvik, Pontus Timberg, Sophia Zackrisson and Anders Tingberg. *Nationellt möte om sjukhusfysik*, Västerås, Sweden, November 2017

1. Introduction and aims

They say, Find a purpose in your life and live it. But, sometimes, it is only after you have lived that you recognize your life had a purpose, and likely one you never had in mind.

Khaled Hosseini, And the Mountains Echoed

Breast cancer is the most common type of cancer among women and more than 8000 individuals are diagnosed each year in Sweden (Socialstyrelsen 2013, Socialstyrelsen 2018). Early detection, diagnosis, and treatment are important for the prognosis, and population-based breast cancer screening programmes have been established in many countries (Giordano *et al.* 2012, Socialstyrelsen 2014, Socialstyrelsen 2015). Today's standard examination method is digital mammography (DM), in which low-energy X-rays are used to generate two-dimensional (2D) images of the compressed breast. Not all breast cancers are detected in DM images (Laming *et al.* 2000), largely due to the superposition of breast tissue, which may hide suspicious findings. Another problem is that the tissue superposition may produce false positive findings. Breast imaging can also be performed with ultrasound, computed tomography (CT), or magnetic resonance imaging (MRI), but none of these modalities have outcompeted DM in screening. However, one imaging technique that might complement or replace DM in future screening programmes is breast tomosynthesis (BT). In BT, an X-ray technique similar to DM, a set of projection images is acquired over a limited angular range and used to reconstruct a volume of slice images. This provides additional information in the third dimension, reducing the problems of breast tissue superposition and increasing cancer detection (Ciatto *et al.* 2013, Skaane *et al.* 2013, Lång *et al.* 2016).

BT image acquisition includes many possible combinations of acquisition parameters, such as angular range, number of projection images, and dose distribution among the projection images (Tingberg *et al.* 2011, Sechopoulos[a] 2013, Poplack 2014). For optimal performance and best clinical outcome, these parameters have to be optimized based on the visibility of breast cancer lesions. Investigating the influence of acquisition parameters on image quality by constructing prototype systems is time-consuming and expensive. Another way of

performing these analyses is with computer simulations (Raeside 1976), in which the parameters may be changed arbitrarily without physical prototype construction or exposing test subjects to radiation.

In addition to increased cancer detection, the reconstructed BT volume could provide information about the distribution of dense tissue within the breast. This is of interest because DM and BT involve ionizing radiation, and the amount and distribution of glandular (dense) tissue affects the radiation dose (Dance *et al.* 2000, Dance *et al.* 2005, Zankl *et al.* 2005, Porras-Chaverri *et al.* 2012, Sechopoulos *et al.* 2012, Geeraert *et al.* 2015). The breast is a radiosensitive organ, and the radiation dose, even though low, should be assessed accurately in order to minimize the risk of inducing cancer (ICRP 2007). By using computer simulations and software breast phantoms, the absorbed dose to glandular tissue can be estimated in a way that is not possible with physical phantoms (Dance *et al.* 2005, Zankl *et al.* 2005, Sechopoulos *et al.* 2012, Geeraert *et al.* 2015). If software phantoms can be generated based on BT volumes, simulations of individual glandular dose could be performed.

The overall aim of this thesis was to develop a simulation procedure for optimizing image acquisition and estimating individual glandular dose in BT.

The specific aims were:

- to develop and validate a simulation procedure for the generation of BT projection images (**Paper I**);
- to investigate the influence of angular range, distribution of projection images, and dose distribution on the visibility of simulated microcalcifications (**Paper II**);
- to verify a method for localizing dense breast tissue using volumetric breast density (VBD) assessment and reconstructed BT volumes (**Paper III**);
- to compare quantitative estimates of VBD based on BT projection images to estimates based on DM images in a large screening cohort (**Paper IV**); and
- to evaluate a method for estimating glandular dose using software breast phantoms based on reconstructed BT volumes (**Paper V**).

2. Background

I don't love studying. I hate studying. I like learning. Learning is beautiful.

Natalie Portman

Breast cancer and mammography

Through the Swedish breast cancer screening programme, women aged 40 to 74 years are invited for regular DM exams (Socialstyrelsen 2014). DM is also used when women are referred for examination due to clinical symptoms, such as lumps, changes in size or shape, and skin or nipple changes, and there is a suspicion of cancer.

Standard DM is a well-established method for examining the breast with the purpose of detecting and diagnosing breast cancer early. The procedure uses low-energy X-rays to generate 2D images of the compressed breast (Figure 1).

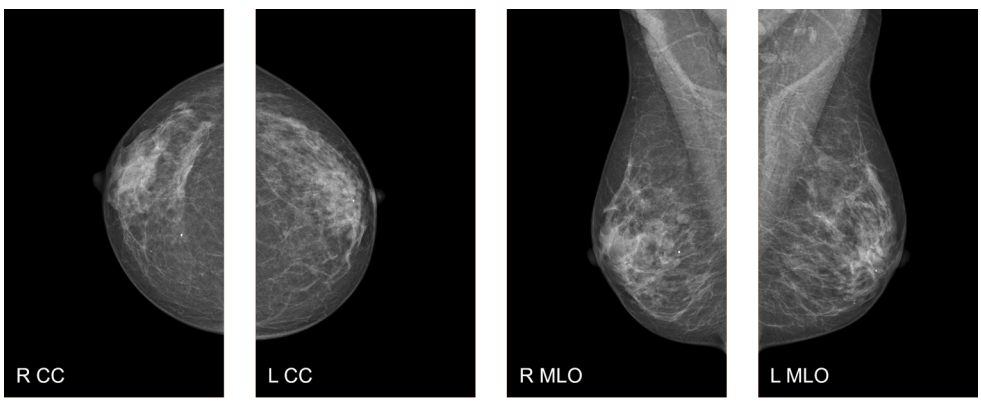

Figure 1.
DM screening includes craniocaudal (CC) and mediolateral oblique (MLO) views of the right (R) and left (L) breast. In a clinical examination in which cancer is suspected, the lateromedial (LM) view is also included (not shown).

During the image reading, a radiologist searches for different types of suspicious findings in the breast, such as microcalcifications, masses, or other structures that

could be signs of cancer (Figure 2). If cancer is suspected, the clinical work-up includes palpation, further imaging with DM, ultrasound in most cases, and MRI in some cases. If the cancer suspicion remains, fine-needle aspiration (involving cytopathology) or core-needle biopsy (involving histopathology) is performed to establish a final diagnosis. In case of a negative result, follow-up in the form of extra DM or ultrasound examinations can be performed if deemed necessary.

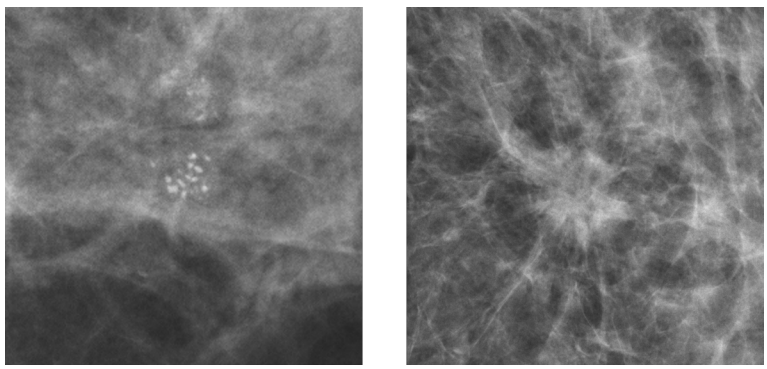

Figure 2.
Examples of suspicious findings in DM images. A cluster of microcalcifications (left) and a spiculated soft tissue mass (right).

Breast density

DM images are based on the variations in X-ray attenuation of the tissues within the breast (Johns *et al.* 1987). Adipose tissue has a lower density and attenuation and appears dark, whereas glandular and connective tissue have higher densities and appear bright in DM images (Figure 3). The sensitivity (proportion of true positive findings) of DM has been shown to be lower and the cancer incidence higher for women with higher amounts of dense tissue (Boyd *et al.* 2010, Boyd *et al.* 2011, Olsson *et al.* 2014). Consequently, breast density could be used as a basis for risk scoring and possible stratification of women for different screening strategies (Howell *et al.* 2014, Evans *et al.* 2015).

Breast density, or the proportion of the breast that consists of dense tissue, is typically expressed as a percentage of the breast area or volume (Yaffe 2008). The value can be estimated qualitatively through different classification systems based on a visual assessment of the breast's radiological appearance (Wolfe[a] 1976, Wolfe[b] 1976, Gram *et al.* 1997, Boyd *et al.* 2011, D'Orsi *et al.* 2013), or quantitatively using computer-assisted methods based on the thresholding of grey level values in the image (Byng *et al.* 1994, Hartman *et al.* 2008, Highnam *et al.* 2010, Geeraert *et al.* 2014). Qualitative measurements, such as Breast Imaging - Reporting and Data System (BI-RADS) scoring (D'Orsi *et al.* 2013), are subjective and associated with

inter-observer variability (Ciatto *et al.* 2005). However, they take tissue patterns and potential masking effects into account, which is important in risk assessment. Quantitative methods have not yet been fully developed for overall risk assessment, but they offer objective estimates of breast density, which could also be useful in breast dosimetry.

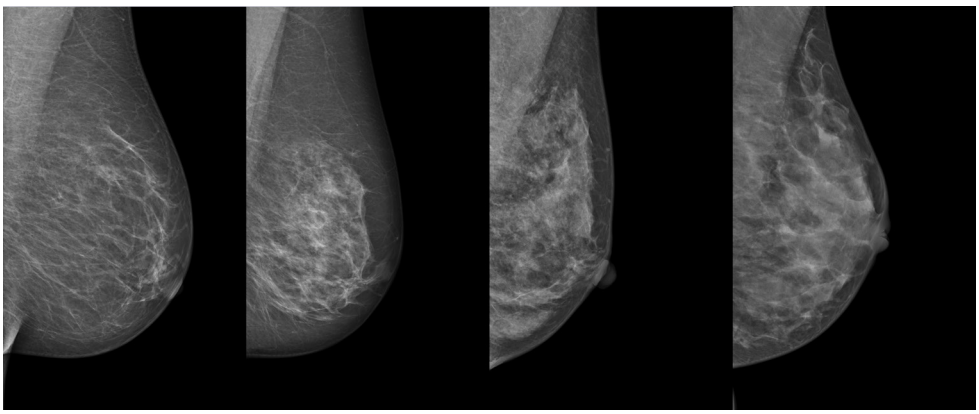

Figure 3.
DM images of breasts with different breast densities, from low (left) to high (right).

Breast dosimetry in mammography

The breast is a radiosensitive organ and mammographic X-ray exposure is associated with an increased cancer risk (ICRP 2007). The vast majority of women participating in breast cancer screening are healthy, and some are relatively young. Therefore, even though the radiation doses associated with DM are low, the absorbed dose to the breast is routinely estimated as part of optimizing the procedure and minimizing the risk of inducing cancer.

The European (Zoetelief *et al.* 1996, Perry *et al.* 2008), UK (Fitzgerald *et al.* 1989, Moore *et al.* 2005), and IAEA (IAEA 2007) protocols present similar methods for breast dosimetry, in which the mean glandular dose for DM, MGD_{DM}, is estimated as Equation 1:

$$MGD_{DM} = K \cdot g \cdot c \cdot s \quad (1)$$

where K is the incident air kerma measured at the upper surface of the breast, and the conversion factors g, c, and s have been derived from computer simulations (Dance 1990, Dance *et al.* 2000, Dance *et al.* 2009). The g-factor converts the incident air kerma to mean glandular dose for the standard breast and is tabulated based on breast thickness and half-value layer (HVL; mm Al). The c-factor corrects

for breasts with different amounts of glandular tissue (breast density) and is tabulated based on breast thickness and HVL for two age groups, assuming age as an indicator of glandularity (Dance *et al.* 2000). The *s*-factor corrects for X-ray spectra with different anode and filter materials and is tabulated for different combinations. The standard breast (Figure 4) is used for the computer simulations, but the incident air kerma is measured to a PMMA phantom for practical reasons (Fitzgerald *et al.* 1989, Dance 1990).

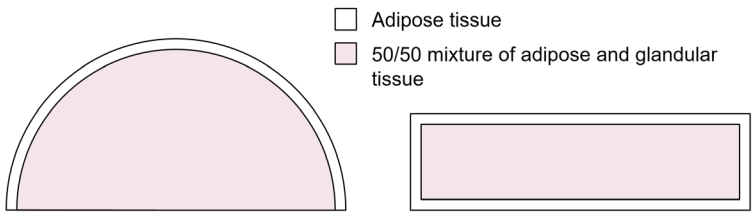

Figure 4.
Cross-sections of the standard breast model with the shape of a 4.5-cm-thick half-cylinder with 16 cm diameter. The phantom has a central region composed of a 50/50 mixture of adipose and glandular tissue and a 0.5-cm-thick outer region of adipose tissue.

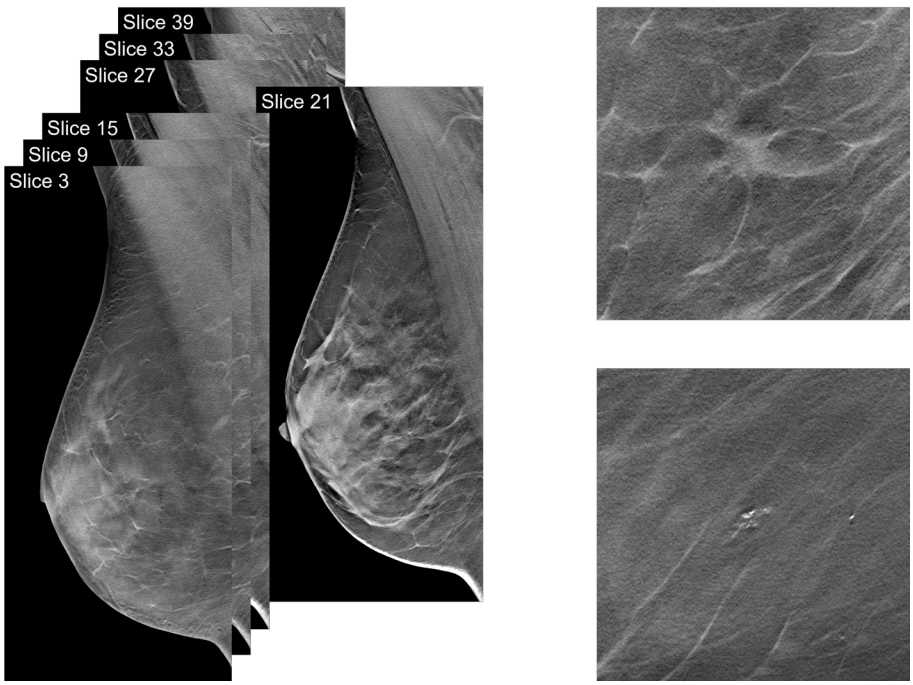

Figure 5.
A reconstructed BT volume acquired in the MLO view (left) and examples of suspicious findings in BT slice images (right): soft tissue mass (top) and a cluster of microcalcifications (bottom).

Breast tomosynthesis

Standard DM images are 2D representations of the three-dimensional (3D) breast. This results in superposition of breast tissue, which may reduce the visibility of lesions (decreased sensitivity) or produce false positive findings when two or more normal structures are superimposed (decreased specificity). To obtain additional information in the third dimension and reduce the problem of superimposed tissue, BT has been introduced as an alternative or complement to standard DM in breast cancer screening (Tingberg *et al.* 2011, Poplack 2014, Lång *et al.* 2016). In BT, low-energy X-rays are used to acquire multiple projection images of the breast over a limited angular range. These images are then reconstructed into a volume of slice images (Figure 5).

Image acquisition

BT image acquisition (Figure 6) can be performed in different ways due to the many possible variations in system geometry and exposure parameters. The BT system can have a narrow or wide angular range, a fixed detector or a detector that rotates with the X-ray tube, and continuous or pulsed (step-and-shoot) exposure delivery (Tingberg *et al.* 2011). Other possible variables are the number of projection images, distribution of projection images, and dose distributions among the projection images (Figure 7).

Generally, the above-mentioned factors can not be varied for a specific BT system, whereas tube voltage, which determines the X-ray spectrum, and radiation exposure (i.e., the number of emitted photons) can be chosen manually or selected automatically by the machine. In clinical use, the tube voltage is determined based on the breast thickness and the radiation exposure through the automatic exposure control (AEC) to generate images with the desired image quality.

The geometry of the BT system and the exposure parameters will more or less affect the image quality of the reconstructed image volume (Sechopoulos[a] 2013). In order to achieve acceptable image quality for the detection of lesions, such as microcalcifications and soft tissue masses, these properties have to be optimized. Manufacturers may choose different solutions based on their technology and compromise between clinical outcome, radiation dose, and recommended guidelines.

Though the acquisition conditions limit the amount of information collected about the breast, the reconstruction method and additional processes (e.g., artefact reduction algorithms) will influence image volume characteristics, such as resolution, noise properties, and artefact appearance (Sechopoulos[b] 2013).

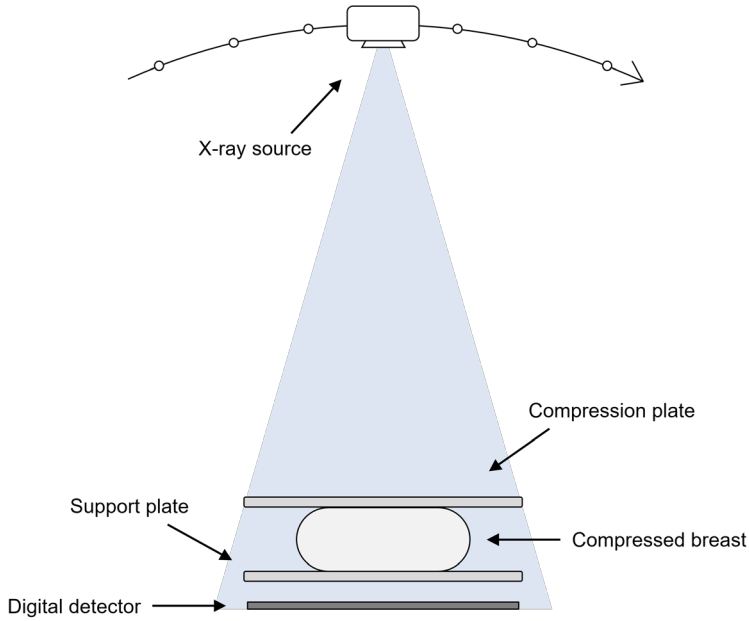

Figure 6.
In BT, the X-ray source moves over a limited angular range while projection images of the breast are acquired by the detector. The breast is compressed between the support and compression plate to immobilize it, reducing motion artefacts, separate structures in the breast, which is especially important in 2D DM, and reduce and equalize the breast thickness, which reduces the effects of scattered radiation, reduces the radiation dose, and enhances the image contrast (Perry *et al.* 2008).

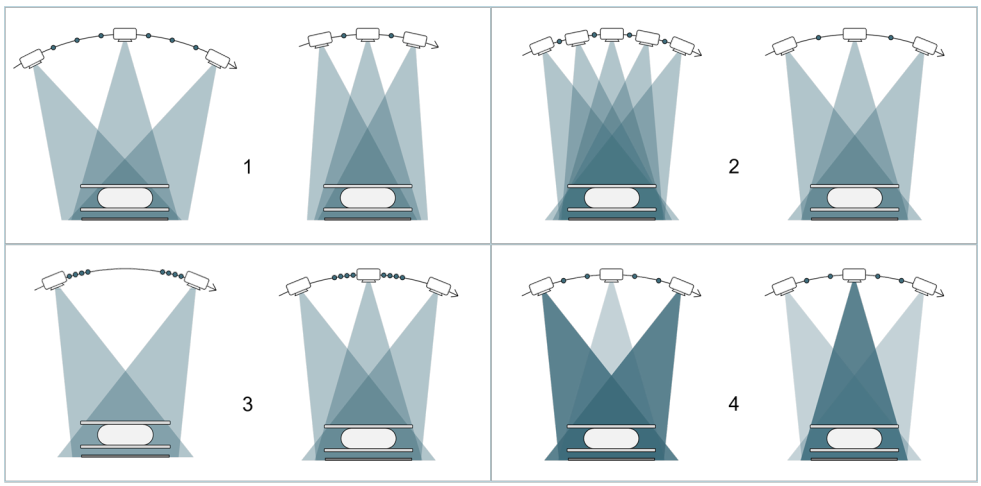

Figure 7.
Examples of variable acquisition parameters for BT. Angular range (1), number of projection images (2), distribution of projection images (3), and dose distribution (4).

Breast dosimetry in breast tomosynthesis

The mean glandular dose for BT, MGD_{BT}, has been proposed to be estimated using the same protocols as DM, with the addition of conversion factors unique to the BT system used (Equation 2):

$$MGD_{BT} = K_T \cdot g \cdot c \cdot s \cdot T \quad (2)$$

where K_T is the incident air kerma measured at the upper surface of the breast for projection angle 0°, but with the total exposure for the examination. The factors *g*, *c*, and *s* are defined in the same way as in Equation 1. The *T*-factor corrects for BT systems with different acquisition geometries and is tabulated based on breast thickness and BT system (Dance *et al.* 2010).

Monte Carlo simulation in X-ray imaging

The outcome of different combinations of BT system geometries and acquisition parameters could be investigated by constructing prototype systems and examining patients or volunteers, but this is time-consuming, expensive, and would involve radiation exposure to multiple test subjects. Another way to perform these analyses is by using computer simulations, which allow the design and acquisition parameters to be altered arbitrarily without physical prototype construction and radiation exposure to humans.

Radiation transport in matter has been studied for a long time. When photons and charge particles with substantial energy, such as electrons and positrons, penetrate matter, multiple interactions occur in which energy is transferred to the atoms and molecules of the material and secondary particles are produced. Theoretical studies of radiation transport are based on the Boltzmann transport equation, which can be solved analytically only under very limited conditions (Harris 1971). With the development and availability of computers, Monte Carlo simulation methods have become an alternative stochastic approach to solving the transport equation and handling radiation transport problems (Berger 1963, Jenkins *et al.* 1988).

Monte Carlo methods are used to solve complex physical or mathematical problems when analytical methods are lacking or too complicated to implement (Raeside 1976). The techniques are based on computational algorithms using stochastic elements to obtain a numerical result. In a Monte Carlo simulation, the sampling of a random number is repeated to reproduce the behaviour of a system or phenomenon (the name refers to gambling at the Monte Carlo Casino).

When simulating radiation transport, the track (or history) of a particle is viewed as a combination of random flights that end with interaction events in which the particle changes direction, loses energy, and sometimes produces secondary particles. The random variables that characterize a flight are the distance between successive interactions, type of interaction, energy loss, angular deflection, and initial state of any secondary particles. By repeated sampling of these variables (from probability distributions determined by interaction mechanisms), flights are generated and particle histories built up. By generating a large enough number of histories, quantitative information about the particle transport may be obtained. The random nature of Monte Carlo methods leads to statistical uncertainties in the achieved result, but the uncertainties can be reduced by increasing the number of simulated histories, which increases the computation time.

The probability distribution functions of the random variables (i.e., travelled distance, type of interaction, energy loss, angular deflection, and secondary particles) are determined by the differential cross-sections of the interaction mechanisms. As the most accurate differential cross-sections available are given in numerical form, extensive databases are incorporated in the advanced Monte Carlo codes.

Monte Carlo simulation of photon transport in complex geometries has been the subject of many studies (Hayward *et al.* 1954, Zerby 1963, Berger *et al.* 1972, Chan *et al.* 1983, Ljungberg *et al.* 1989). For photons in the energy range of 50 eV up to 1 GeV, the dominant interaction processes are the photoelectric effect (photoelectric absorption), coherent (Rayleigh) scattering, incoherent (Compton) scattering, and electron-positron pair production (Hubbell *et al.* 1980, Hubbell 1982, Seltzer 1993) (Figure 8).

In photoelectric absorption, a photon of energy E and direction angle θ is absorbed by the target atom, which moves into an excited state and emits an electron with energy E_e and direction angle θ_e. Fluorescence may occur when the atom returns to its ground state. Rayleigh scattering is the process in which the incident photon (E, θ) is scattered by a bound atomic electron without excitation of the target atom. The scattered photon has the same energy E but a new direction angle θ'. In Compton scattering, the incident photon (E, θ) interacts with an electron in the target atom. The photon is absorbed, a new photon (E', θ') is emitted, and the electron recoils with energy E_e and direction angle θ_e. Lastly, electron-positron pair production may occur if the photon (E, θ) has an energy >1.022 MeV (twice the electron rest energy). The photon passes near the nucleus (or an electron) of the target atom and is absorbed, and an electron (E_e, θ_e) and positron (E_p, θ_p) are created.

The probability of the different interactions occurring depends on the atomic number (Z) of the material and the photon energy. For the X-ray energies in DM and BT (up to ~35 keV), photoelectric absorption and Compton scattering are the

dominant interaction mechanisms in low Z materials, such as tissue (electron-positron pair production does not occur).

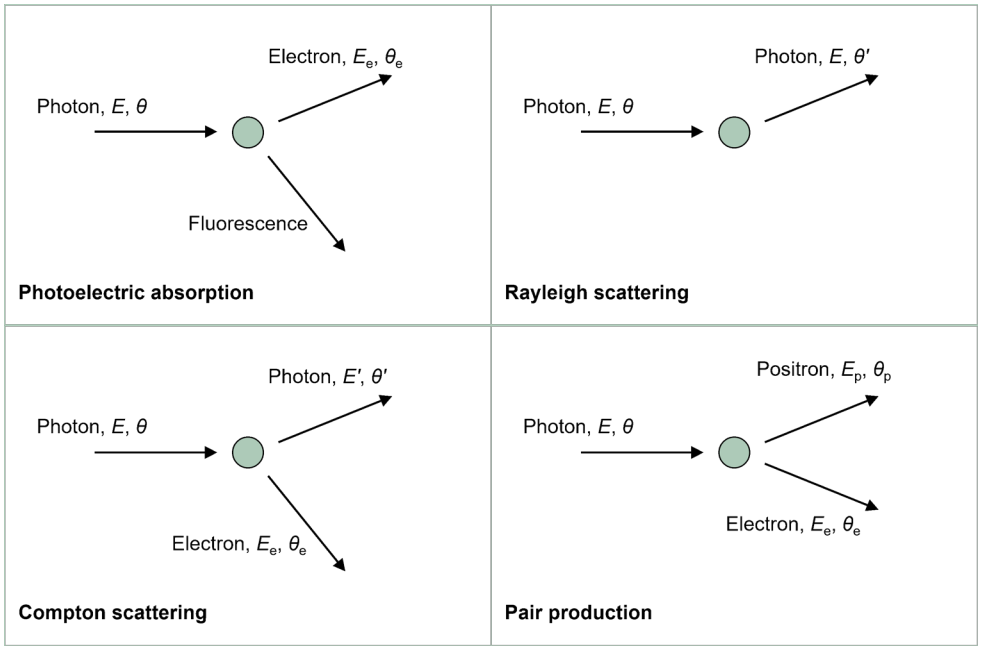

Figure 8.
Basic photon interactions with matter. A photon with energy E and direction angle θ incident from the left at a target atom (green). The interactions involve absorption, energy loss, angular deflection, and/or production of secondary particles.

3. Simulation procedure

When you realize there is something you don't understand, then you're generally on the right path to understanding all kinds of things.

Jostein Gaarder, The Solitaire Mystery

A Monte Carlo simulation procedure was developed to investigate the acquisition geometry of a BT system. The procedure, which is described in this chapter and further in **Paper I**, uses a combination of analytical ray tracing, Monte Carlo simulation, and measured values from flat field image acquisitions to generate BT projection images of software breast phantoms (Figure 9). The simulation procedure can also be used to estimate local energy deposition in glandular tissue to calculate absorbed glandular dose.

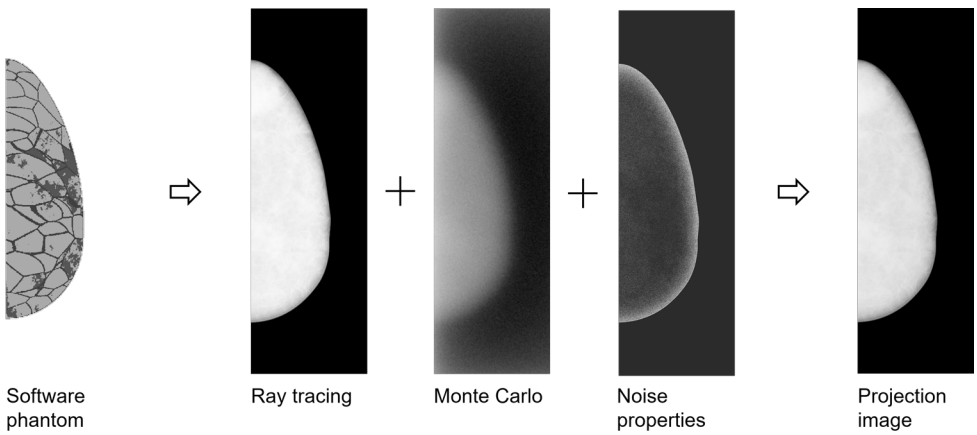

Figure 9.
Generation of BT projection images of software phantoms. The developed simulation procedure uses analytical ray tracing to model primary photons, Monte Carlo simulaiton to model scatter contribution, and flat field image acquisitions to estimate noise and system properties. The energy deposition in glandular tissue is scored during the Monte Carlo simulation step.

Monte Carlo program: PENELOPE

Several Monte Carlo code packages are available for simulations in diagnostic medical imaging research. EGSnrc (Rogers *et al.* 1995, Kawrakow 2000), GEANT4 (Agostinelli *et al.* 2003, Allison *et al.* 2006), MCNPX (Pelowitz *et al.* 2011), and PENELOPE (Sempau *et al.* 1997, Salvat *et al.* 2001, Sempau *et al.* 2003) are four commonly used and well-established packages that are continuously being developed. For the purpose of simulating BT image acquisition and absorbed dose, the PENELOPE code package was chosen based on its currently free and open software, which is applicable down to very low energies, and the implemented image detector necessary for image generation. In addition, the PENELOPE code package is well documented and actively maintained. (The choice of this Monte Carlo package does not mean that other packages would have been less suited for the task.)

To operate PENELOPE and its subroutines, a main program is used together with input files describing the geometry, material characteristics, and simulation parameters as described below.

Main program and execution platform

The developed simulation procedure utilizes the simulation tool penEasy Imaging[2] (version 2010-09-02), an extension of the penEasy main program (version 2008-06-15) (Sempau *et al.* 2011). It uses the atomic physics modelling subroutines from PENELOPE 2006. At the moment, the source code and documentation of penEasy Imaging are open and free and can be obtained at the website http://code.google.com/p/peneasy-imaging.

The simulations are executed in a UNIX environment (64-bit Ubuntu 11.10) on a personal computer with an Intel Core i7-3960X 3.30 GHz processor and 64 GB RAM. The six core CPU allows for up to 12 simulations to be run simultaneously through 12 virtual cores, and the relatively large RAM was necessary for the large data files describing the software phantoms.

Geometry and material definition

The objects in the simulation geometry are stated in a separate text file as homogenous bodies limited by quadric surfaces. The geometry can be visualized

[2] penEasy Imaging was developed at the U. S. Food and Drug Administration (FDA) Center for Devices and Radiological Health, Office of Science and Engineering Laboratories, Division of Imaging and Applied Mathematics.

using gview2d (Figure 10), a Microsoft Windows software tool included in the PENELOPE distribution. To describe bodies of inhomogeneous material or arbitrary free-form objects, such as anatomic structures, voxel geometries are used (see section: Software breast phantom). The simulation geometry may be described by quadrics only, by voxels only, or through a combination in which a material in the quadric geometry is made transparent for the voxel geometry.

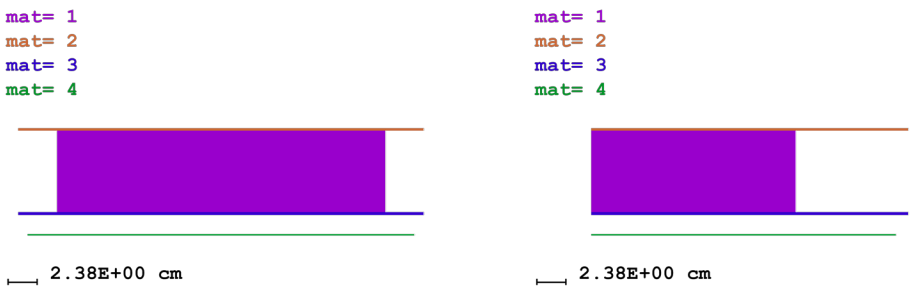

Figure 10.
A box-shaped phantom (material 1) between the compression plate (material 2) and the support plate (material 3) above the image detector (material 4). Front view (left) and side view (right) displayed by the auxiliary program gview2d. A material, such as material 1, may be made transparent and replaced with a voxel geometry.

The required physical information for each material present in the simulation geometry (Table 1) is read from a material data file. The material files are most easily prepared by the auxiliary program MATERIAL, which is included in the distribution package. In addition to the 280 predefined materials, arbitrary materials can be prepared by entering the necessary information.

Table 1. Simulation materials
Objects and materials used in different simulation geometries.

OBJECT	MATERIAL	DENSITY (g/cm^3)
Compression plate	PET	1.40
Block phantom	PMMA	1.19
Support plate	Graphite	1.70
Surrounding air	Air, dry (near sea level)	0.001205
Aluminium foil	Aluminium	2.79
Gold disc	Gold	19.32
Adipose tissue	Adipose tissue (Snyder *et al.* 1975)	0.920
Glandular tissue	Glandular tissue (Woodard *et al.* 1986)	1.06
Cooper's ligaments	Glandular tissue (Woodard *et al.* 1986)	1.06
Skin	Skin (Snyder *et al.* 1975)	1.10
Microcalcifications	Calcium oxalate (Fandos-Morera *et al.* 1988, Shaheen *et al.* 2011)	2.12
Soft tissue mass	Glandular tissue (Woodard *et al.* 1986)	1.06

Simulation parameters

The parameters controlling the simulation are specified in the input data file. Important parameters are number of simulated histories (emitted particles), simulation time, source model, geometry and material files, scored quantities (e.g., energy deposition), and variance reduction methods (not applied in the presented simulation procedure).

The simulation is limited by the number of histories or simulation time, whichever comes first. This has a large impact on simulation results and should be large enough to yield low statistical uncertainties in the scored quantities (Figure 11 and Figure 12).

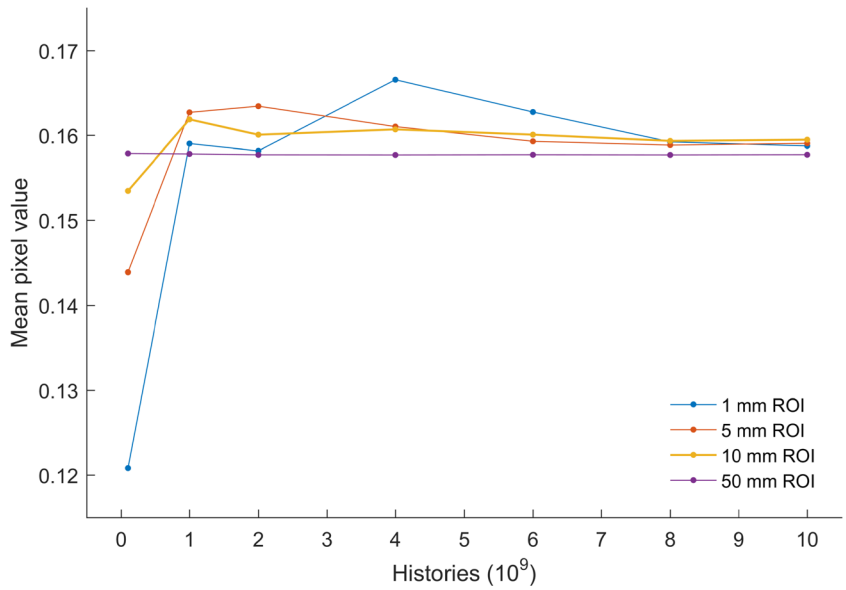

Figure 11.
ROI measurements of scatter contribution in radiographic images (45 mm PMMA, pixel size 0.5×0.5 mm^2) simulated with different numbers of histories. For a large ROI of 50 mm, the mean pixel value is almost constant for the simulated histories. For smaller ROIs, the number of simulated histories should be higher to yield a low uncertainty in the result. Note that the *y*-axis does not include zero.

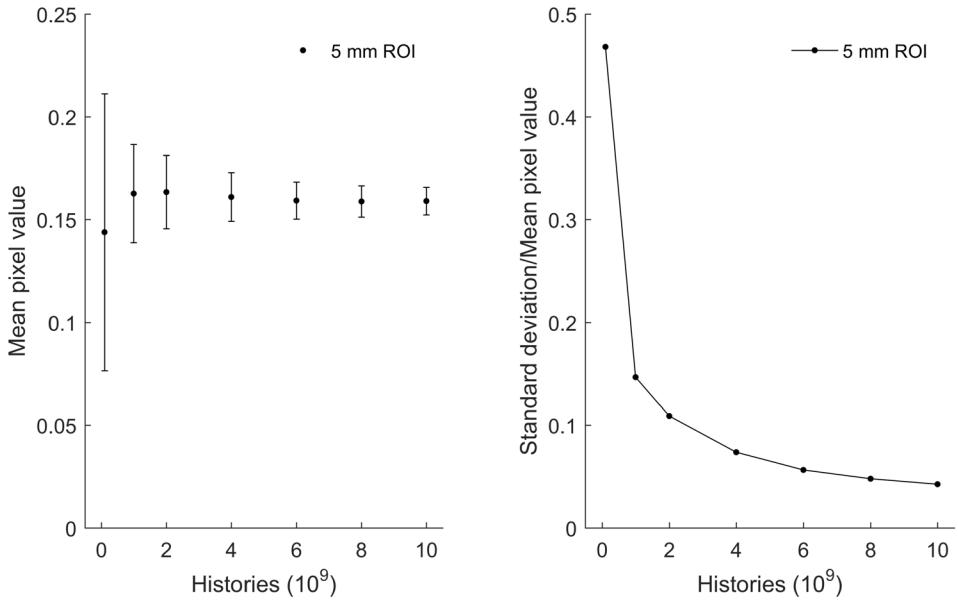

Figure 12.
ROI measurements of scatter contribution in radiographic images (45 mm PMMA, pixel size 0.5×0.5 mm^2) simulated with different numbers of histories. Left: Data are presented as the mean value and standard deviation for a 5 mm ROI. Right: Relative uncertainty in the mean pixel value of a 5 mm ROI for different numbers of histories.

In addition to the subroutines of penEasy, an extra source model, penEasy_Imaging, offers a tally for the generation of radiographic images. For the generation of BT projection images, this tally is used in two ways. To estimate the contribution from primary photons (photons reaching the detector without undergoing any interactions), scatter- and noise-free images are generated through analytical ray tracing. Nine rays are directed at each detector pixel and the output image presented in eV/cm^2 per history, scaled by the probability of particle emission within the solid angle covering each pixel. To estimate the contribution from scattered photons (Rayleigh, Compton, and multiple scattered photons), the energy deposition (eV/cm^2 per history) in each detector pixel is scored separately for primary and scattered particles thorough Monte Carlo simulation.

Modelled breast tomosynthesis system

The simulation procedure was designed to generate projection images from a MAMMOMAT Inspiration BT system (Siemens Healthcare GmbH, Forchheim, Germany).

Acquisition geometry and X-ray spectra

The modelled BT system (Figure 13) acquires 25 projection images over an angular range of 50 degrees. Continuous tube motion over a 20 s scan time, with an approximate 100 ms exposure time per projection, results in a focal spot movement of 2.7 mm in the direction of the tube motion (Figure 14). System-specific photon energy spectra for tube voltages between 25 and 32 kV and W/Rh anode/filter combination are used in the simulations (Boone 1998) (Figure 15).

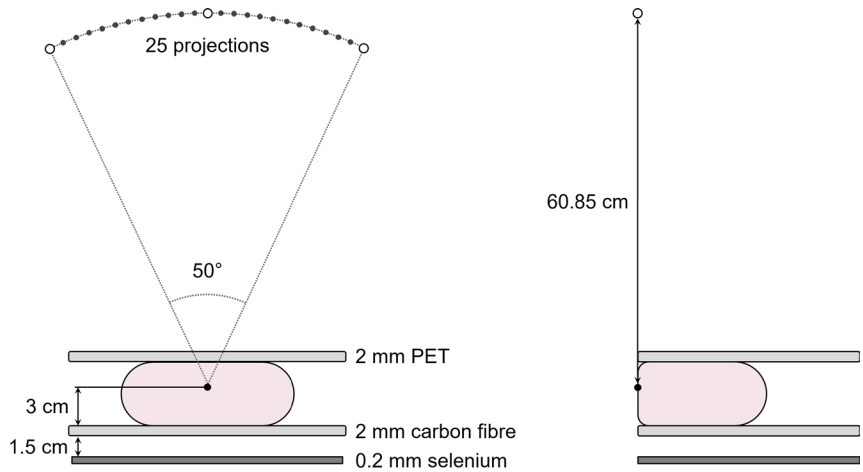

Figure 13.
Geometry of the modelled BT system. The centre of rotation is placed at the chest wall side 60.85 cm below the X-ray source and 3 cm above the support plate.

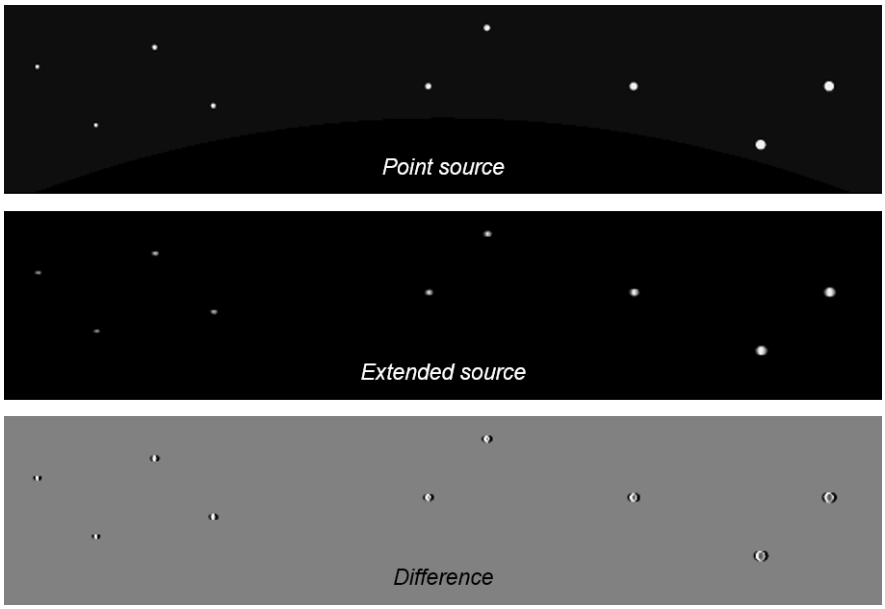

Figure 14.
Ray-traced projection images of an aluminium strip with gold discs (small part of a CDMAM phantom) showing the effect of 2.7-mm focal spot movement in the direction of the tube motion. While Monte Carlo simulation is performed for an extended source, ray tracing is performed for a point source. To take the focal spot movement into account in the ray tracing, the latter was performed for five source positions spread over 2.7 mm for each projection angle.

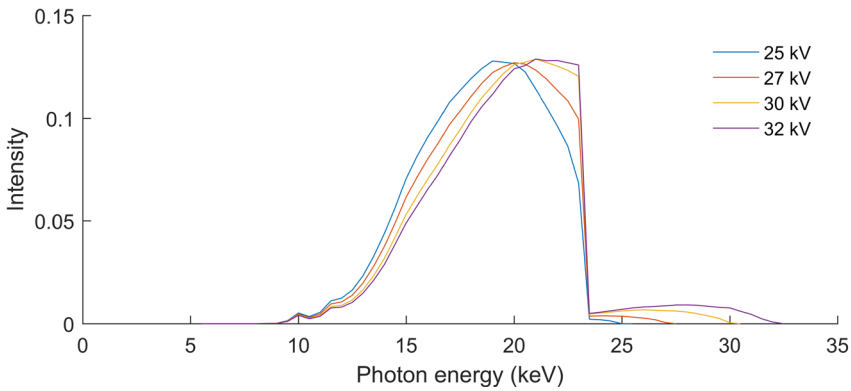

Figure 15.
Examples of system-specific photon energy spectra for W/Rh anode/filter combination. While Monte Carlo simulation is performed for a whole spectrum, ray tracing is performed for only one photon energy. To take the photon energy spectrum into account in the ray tracing, the latter was performed for 10 photon energies.

The BT system has a solid-state detector comprising 0.2-mm-thick amorphous selenium with a pixel size of 85×85 μm^2. In the simulation procedure, the detector is modelled as a perfect energy integrating detector (Smans *et al.* 2010). The noise contribution is estimated from flat field images acquired under conditions similar to the simulation conditions (i.e., dose level, tube voltage, and homogenous phantom material and thickness) (Svalkvist *et al.* 2010). For a simulated image, the normalized noise power spectrum of the corresponding flat field image is used to generate a noise image with the same frequency components but a random appearance. The noise image is corrected for local dose variations in the simulated image by estimating the standard deviation as a function of the mean value from flat field images (Figure 16).

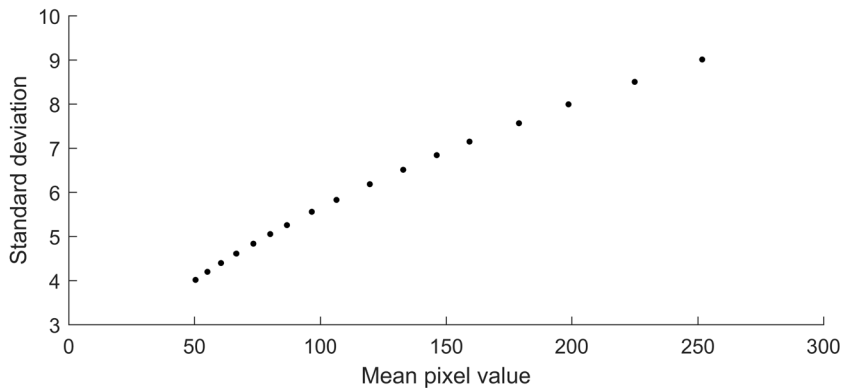

Figure 16.
The standard deviation as a function of the mean value of a centrally positioned ROI for flat field images acquired at different dose levels using the same tube voltage (28 kV) and PMMA thickness (45 mm).

Reconstruction method

Different methods can be used to reconstruct BT volumes from the simulated projection images. The previous standard reconstruction method, standard filtered back-projection (FBP) (Lauritsch *et al.* 1998, Mertelmeier *et al.* 2006, Orman *et al.* 2006), is being replaced by super-resolution reconstruction with statistical artefact reduction (SRSAR or Siemens EMPIRE) (Abdurahman *et al.* 2012, Abdurahman *et al.* 2014). Instead of using a slice-thickness filter (Mertelmeier *et al.* 2006, Orman *et al.* 2006), SRSAR reconstructs the volume into very thin slices and removes artefacts using an outlier detection algorithm. To reduce the increased image noise, the thin slices are collapsed into thicker slices, after which an iterative edge and microcalcification-preserving filtering scheme is applied.

Software breast phantom

The breast software model used in the simulation procedure was developed at the University of Pennsylvania (Bakic *et al.* 2011). The breast phantom contains voxels with values representing skin, Cooper's ligament, glandular tissue, adipose tissue, and surrounding air (Figure 17). By changing the voxel values, the phantom is modified into different glandularities and distributions of glandular tissue. Lesions, such as microcalcifications, can be inserted following the same procedure.

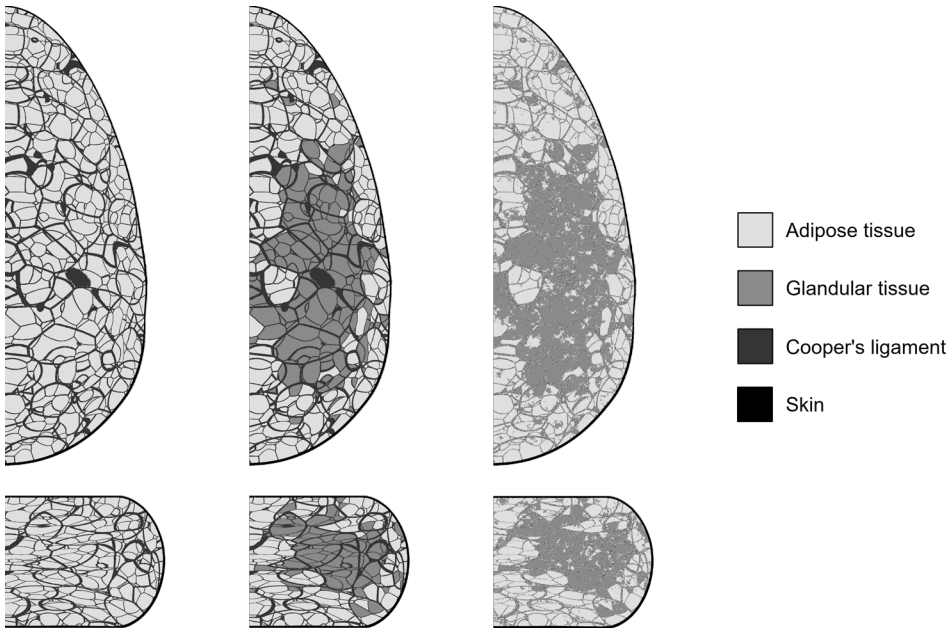

Figure 17.
Axial and mid-sagittal cross-sections of the software breast phantom. The modelled breast compressed for the MLO view with a size of 25.90×8.05 cm^2 and a compressed breast thickness of 6.37 cm (left). A number of compartments are filled with glandular tissue (middle) and the phantom modified to contain heterogeneous regions of adipose and glandular tissue (right).

Breast density estimation

For software phantoms, the breast composition is known and the breast density (or glandularity) can be calculated easily as the ratio between the amount of glandular tissue and the total amount of breast tissue (by volume or weight and with or without the skin). For screening or clinical cases, in which the details about the individual breast composition is not known, there are methods for estimating breast density from the central BT projection image similarly to DM (van Engeland *et al.* 2006,

Hartman *et al.* 2008, Highnam *et al.* 2010, Geeraert *et al.* 2014, Pertuz *et al.* 2015, Machida *et al.* 2016).

For the BT system modelled in the simulation procedure, prototype software (Siemens VBDA 1.3.0, not commercially available) is being developed (Fieselmann *et al.* 2016). To estimate volumetric breast density (VBD), a physics model of the image acquisition process is used with the assumption that the breast consists of fatty and glandular tissue with known energy-dependent X-ray attenuation values. The amount of glandular tissue located above each detector pixel is calculated and compiled into a 2D density map (Figure 18), from which the total amount of glandular tissue and VBD are estimated. The model also addresses the masking effect of soft tissue masses for dense tissue areas to mimic the qualitative BI-RADS scoring (D'Orsi *et al.* 2013).

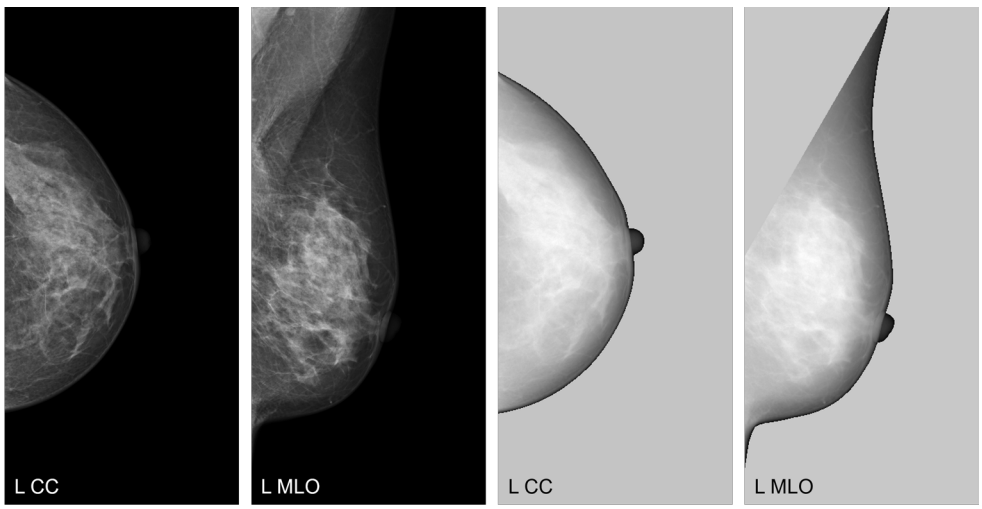

Figure 18.
Examples of DM images (left) and corresponding breast density maps (right) (kindly provided by Andreas Fieselmann, Siemens Healthcare GmbH, Forchheim, Germany). Note that the figure shows processed DM images while the VBDA software (Fieselmann *et al.* 2016) is applied to unprocessed images.

4. Paper summaries

The developed simulation procedure (Chapter 3: Simulation procedure) was validated in **Paper I**. In **Paper II**, the procedure was used to investigate the influence of different acquisition schemes on the visibility of simulated microcalcifications in reconstructed BT volumes. In **Paper III**, the procedure was used to verify a method for localising glandular tissue using BT data. Breast density based on BT images, which is important for dense tissue localization and glandular dose estimates, was estimated in **Paper IV** by prototype software and compared to estimates based on DM images. In **Paper V**, a method for estimating glandular dose using the developed simulation procedure and software breast phantoms based on reconstructed BT volumes was evaluated.

Paper I

Validation of a simulation procedure for generating breast tomosynthesis projection images

In **Paper I**, the simulation procedure was validated by comparing contrast and sharpness in simulated images to real images acquired with the modelled BT system. The validation method included contrast detail test objects used in routine quality control of DM and BT systems (Elangovan *et al.* 2014).

To compare contrast, a square piece of aluminium foil was imaged with PMMA thicknesses of 30 to 70 mm and AEC, corresponding to tube voltages from 27 to 31 kV and various exposures. The same conditions were used when generating BT projection images with the simulation procedure. The signal-difference-to-noise ratio (SDNR) for aluminium and background was calculated and compared for the real and simulated projection images. In addition, the normalized noise power spectrum (NNPS) was measured to compare image noise.

To compare sharpness, the degradation of contrast with object size was estimated from a small part of a CDMAM phantom containing an aluminium strip with gold discs of different sizes (Warren *et al.* 2013). The test object was placed on top of and below 45 mm of PMMA and imaged at 29 kV and a high exposure setting. The same conditions were used in the simulation. The contrast degradation factor (CDF)

was calculated for seven disc sizes in the real and simulated reconstructed image volumes (Elangovan *et al.* 2014).

The SDNR was found to be higher in the simulated projection images for all PMMA thicknesses. Though the background values showed good agreement, the signal values (aluminium region) were consistently lower in the simulated images. The NNPS indicated a good relationship between noise properties and a moderate agreement of noise levels. The CDF data showed good agreement for real and simulated reconstructed images.

In conclusion, the results of the validation indicated that the simulation procedure can be used to generate BT images with realistic sharpness but higher image noise and contrast than experimentally acquired images.

Paper II

Monte Carlo simulation of breast tomosynthesis: visibility of microcalcifications at different acquisition schemes

The purpose of **Paper II** was to investigate the influence of BT acquisitions with different angular ranges, projection distributions, and dose distributions on the visibility of simulated microcalcifications in reconstructed image volumes.

Microcalcifications ($150\times150\times150$ μm^3) were inserted at 100 random positions in a high-resolution software breast phantom (Bakic *et al.* 2011) and the simulation procedure used to generate BT projection images with 10 different acquisition schemes (Figure 19). The projection images were used to reconstruct image volumes with the new SRSAR reconstruction method. For comparison purposes, the volume of the standard acquisition scheme (50°, uniform dose) was also reconstructed using the previous standard reconstruction method, standard FBP.

To evaluate the contrast (in-plane visibility) and depth resolution, the SDNR and artefact spread function width (ASFW) of the microcalcifications were calculated for the different acquisition schemes. The standard FBP reconstruction of the standard acquisition (50°, uniform dose) yielded significantly lower mean SDNR (i.e., lower contrast) and higher mean ASFW (i.e., lower depth resolution) than the reconstructions made with SRSAR. The mean SDNR was significantly lower for the acquisition schemes with very high central dose than for the acquisition schemes with more uniform dose distributions. The mean ASFW was lowest for the acquisition schemes with an angular range of 50° and increased with narrower angular ranges. Ten out of the 100 microcalcifications were not discernible in all reconstructed volumes and were excluded from the ASFW estimates.

The conclusion of the study was that none of the evaluated acquisition schemes yielded higher SDNR or depth resolution for simulated microcalcifications than the standard acquisition scheme (50° angular range, uniform projection and dose distribution). Furthermore, the new SRSAR reconstruction method outperformed standard FPB in both SDNR and depth resolution.

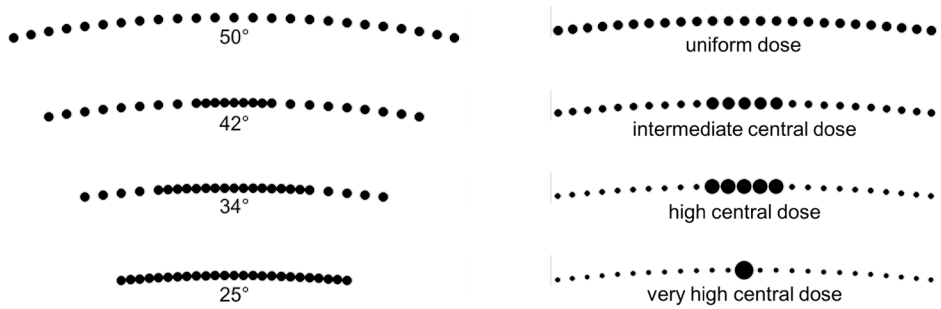

Figure 19.
The investigated acquisition schemes had different angular ranges, projection distributions, and dose distributions. All schemes included 25 projections and a total exposure of 127 mAs. For an angular range of 50° and 25°, the projections were evenly distributed with an angular increment of 2° and 1°, respectively. These projection distributions were evaluated for uniform dose (5.1 mAs/projection), intermediate central dose (10.1 versus 3.8 mAs/projection), high central dose (12.7 versus 3.2 mAs/projection), and very high central dose (63.4 versus 2.6 mAs/projection). For an angular range of 42° and 34°, the outer projections had a 2° increment and the central projections a 1° increment. These projection distributions were only evaluated for a uniform dose distribution (5.1 mAs/projection).

Paper III

Volumetric localisation of dense breast tissue using breast tomosynthesis data

Paper III combined data from the reconstructed BT volume and density estimation from the central projection images in order to localize the dense tissue. To verify the method, the simulation procedure was used to generate BT projection images of software breast volumes.

Five binary software volumes with random, breast tissue-like structures were generated based on fractal Perlin noise (Dustler *et al.* 2015) and BT projection images simulated. With the assumption that the breast consists of two tissue types (fatty and dense tissue) with different attenuation properties, the amount of dense tissue could be estimated from the central BT projection image (van Engeland *et al.* 2006). For each of the five phantoms, a BT volume was reconstructed and scaled to the size of the original breast phantom. Based on the density map and the voxel

intensities, the voxels were assigned as dense or fatty, creating a binary volume similar to the original phantom.

The recreated phantom was compared to the corresponding original phantom in regards to the amount of dense tissue and number of correctly assigned voxels. The mean volumetric density estimated for the recreated phantoms was 77 ± 12% of the original volumetric density, and the mean proportion of accurately localized voxels was 75 ± 5%. From this result, the amount and location of dense tissue within the breast can be approximately estimated using BT data.

Paper IV

Comparison between software volumetric breast density estimates in breast tomosynthesis and digital mammography images in a large public screening cohort

In **Paper IV**, software estimates of VBD based on central BT projection images were compared to estimates based on DM images in a large screening cohort. The VBD estimates were also compared to BI-RADS (D'Orsi *et al.* 2013) density scores made by radiologists.

DM and BT images for 9909 women from the Malmö Breast Tomosynthesis Screening Trial (MBTST) (Lång *et al.* 2016) were analysed retrospectively by prototype software (Siemens VBDA 1.3.0, not commercially available) (Fieselmann *et al.* 2016) to estimate VBD. For BT, the VBD was estimated using the central raw projection image for the MLO view. For DM, the VBD was estimated using the raw image for the MLO and CC view. BI-RADS density scoring based on the DM images had been performed as a part of the MBTST. The VBD was compared between one-view BT (MLO) and two-view DM (MLO and CC) and to the radiologists' BI-RADS density scores.

VBD was estimated to be slightly higher in DM images than in BT images, but there was a high correlation between VBD in DM and BT. The distribution of density categories differed slightly between software calculations in DM and BT, but there was substantial agreement. Furthermore, there was moderate agreement between the radiologists' BI-RADS scores in DM and software density categories in DM and BT.

The results indicated that the prototype software may be used for automatic and objective estimates of VBD in BT, with similar performance as DM. This is valuable for risk scoring and individualized screening purposes, especially if BT were to replace DM in breast cancer screening.

Paper V

Breast dosimetry simulation using software phantoms and volumetric localization of glandular breast tissue from reconstructed breast tomosynthesis volumes

The aim of **Paper V** was to evaluate a method for estimating glandular dose using software breast phantoms recreated from reconstructed BT volumes. The method included generation of BT projection images through the simulation procedure described in **Paper I** and volumetric localization of glandular tissue based on BT data.

A detailed software breast phantom (Bakic *et al.* 2011) was modified into 36 versions with different glandularities (10 or 15%) and distributions of glandular tissue (bottom, middle, or top). The simulation procedure was used to generate BT projection images of the phantoms, and BT volumes were reconstructed. The glandular tissue was segmented iteratively based on the glandularity of the corresponding original phantom by changing the threshold value while identifying the connected components in the BT volumes. The segmented image volumes were converted to voxel volumes with the same size and material values as the original breast phantoms. The simulation procedure was used to estimate the glandular dose per unit incident air kerma (for projection angle 0°) for the original and recreated breast phantoms.

Comparing the voxel values, 84 ± 5% of the glandular voxels in the recreated phantoms (mean value and standard deviation for the 36 phantoms) were placed within 1 mm of the glandular voxels in the original phantoms. The glandular dose per unit incident air kerma differed with glandular distribution (i.e., higher glandular dose for top distributions and lower dose for bottom distributions) for phantoms with both 10 and 15% glandularity. The overall accuracy was good for estimating glandular dose with breast phantoms recreated from reconstructed BT volumes. The mean relative differences between the original and recreated phantoms ranged from –0.15 ± 0.05 (15%, bottom) to 0.18 ± 0.13 (15%, top), but apart from three phantoms with 15% glandularity placed in the top of the breast, relative differences were less than 0.2 for all phantoms.

In conclusion, with access to BT volume and prior knowledge of glandularity, the glandular dose per incident air kerma was estimated with good overall accuracy for breast phantoms with different glandularities and glandular distributions. If the method was developed for human cases, it could be a useful tool for estimating individual glandular dose or other quantities related to breast dosimetry.

5. Discussion

Och under dagar som kom gjorde Ronja inget annat än aktade sej för det som var farligt och övade sej att inte vara rädd. Trilla i älven skulle hon akta sej för, hade Mattis sagt, därför skuttade hon med liv och lust på de hala stenarna vid älvkanten, där det brusade som allra värst. Inte kunde hon gå borta i skogen och akta sej för att trilla i älven. Skulle det vara någon nytta med det, så måste det ju ske vid forsarna och ingen annan stans.

Astrid Lindgren, Ronja Rövardotter

Evaluation of simulation procedure

The developed simulation procedure (Chapter 3: Simulation procedure) was validated in **Paper I**. The simulated BT projection images had realistic sharpness but higher contrast than the experimentally acquired images. Several possible causes for this are discussed in **Paper I**, and the simplification of the X-ray spectrum may be an important factor. As the ray tracing is a weighted mean of 10 photon energies instead of the entire spectrum, this could affect the signal in the image. Even though the SDNR values were substantially higher for simulated images than for real images, this increase could be traced to relatively small differences in signal values (up to 5%).

The procedure could probably be improved to generate images with SDNR and NNPS values more similar to those of real images. However, this is not necessarily desirable if it means a large increase in simulation time and/or cost. The projection images generated by the simulation procedure were considered realistic enough for relative quantitative assessments of image quality factors, such as contrast and SDNR, to evaluate acquisition parameters. The procedure could also be useful in developing methods for dense tissue localization and absorbed dose estimation, applications that do not rely strongly on the detailed image characteristics. For the images to be used for qualitative assessments and observer studies with radiologist readers, the realism of the breast phantom has to be considered. Even if there are methods for improving the realism of software phantoms (Dustler *et al.* 2015), the breast tissue background is not identical to that of a real breast. Therefore, it may

not yet be feasible to use simulated images for observer studies of detection and diagnostic accuracy.

Acquisition geometry of breast tomosynthesis

No consensus is currently available among BT manufacturers about the ideal acquisition geometry for breast cancer detection. One reason for this may be the fundamental difference in imaging characteristics between microcalcifications and soft tissue masses, both of which are common suspicious findings in breast cancer screening. Microcalcifications may be very small with high density and attenuation compared to breast tissue. Soft tissue masses are larger with almost the same attenuation properties as glandular tissue. Therefore, different approaches may be favourable for imaging different structures and manufacturers may aim to solve the same problem with different theories and methods, with patents as a limiting factor. The outcome is not only manufacturer- and technology-dependent, but also a compromise between image quality, radiation dose, and practice guidelines.

In **Paper II**, the simulation procedure was used to evaluate the visibility and depth resolution of microcalcifications for 10 BT acquisition schemes with different angular ranges, projection distributions, and dose distributions. The results showed that the acquisition schemes with very high central dose yielded significantly lower SDNR than the schemes with more uniform dose distributions, and the depth resolution increased with wider angular range. This agrees, to some extent, with earlier studies (Sechopoulos[a] 2013), but direct comparisons are difficult due to large differences in the study design.

Though there is more evidence to support that a wide angular range will favour the imaging of soft tissue lesions (Sechopoulos[a] 2013), it is not obvious that the same applies for small microcalcifications. A wider angular range increases the depth information and decreases superposition of the tissue, which may increase the contrast of structures within a slice image. However, microcalcifications often appear in clusters and detection might be aided by an increased slice thickness, resulting in more of the cluster being visible in the same slice image. Depending on the reconstruction method, the slice thickness can be varied.

The results of **Paper II** indicate that the standard acquisition scheme (50° angular range and uniform projection and dose distribution) is favourable the visualization of single 100-µm microcalcifications by the modelled BT system. This outcome may not be valid for microcalcifications of other sizes or for other BT systems. It is also clear from the investigation that the choice of reconstruction method is important for the measurement outcome. However, this does not necessarily limit the applicability of the results, as the choice of reconstruction method may not be

critical for the optimization of acquisition parameters (Zeng *et al.* 2015, Zeng *et al.* 2017).

Localization of glandular tissue and estimation of breast density

If BT becomes the standard modality in breast cancer screening, the improved depth resolution can be used for more than improved cancer detection. For example, VBD assessment and 3D localization of dense breast tissue is important for improved lesion insertion methods to evaluate image quality and for estimating individual glandular dose more accurately.

The limited BT acquisition angle means that the depth resolution is much lower than the in-plane resolution, and BT slice image values are not convertible into Hounsfield units as in CT. In addition, the attenuation properties of adipose and glandular tissue are similar; therefore, it is challenging to segment and localize the dense breast tissue in the BT volume. However, the method described in **Paper III** could accurately localize approximately 75% of the voxels. The model included only a smaller volume of simulated breast tissue-like appearance and not a complete breast phantom with different structures and skin, but the result is still an indication that it is possible to estimate the location of dense tissue within the breast using BT data. As the method's estimation of breast density was approximately 77% of the original amount, it could be argued that more voxels may be correctly localized if this estimation was improved.

In **Paper IV**, an automatic and objective way of estimating VBD in BT was evaluated relative to DM. The used software is valuable for improving methods of dense tissue localization, as well as risk scoring and individualized screening purposes, especially if BT is to replace DM in breast cancer screening. The evaluation did not include a comparison against true VBD values or the gold standard (presumably MRI). However, another evaluation using breast tissue equivalent phantoms has shown that the software accurately and reproducibly measures VBD (Fieselmann *et al.* 2018).

Assessment of individual glandular dose

With current dosimetry protocols (Fitzgerald *et al.* 1989, Zoetelief *et al.* 1996, Moore *et al.* 2005, IAEA 2007, Perry *et al.* 2008), the calculation of MGD does not take into account the individual glandularity (breast density or VBD) or glandular

distribution. Therefore, it may not provide a good measure of the individual radiation dose, which may be important as a basis for risk communication and possible future calculation of accumulated exposure. BT provides information on the tissue distribution in 3D and the reconstructed BT volume may be used for localization of glandular tissue (**Paper III**), whereas the central BT projection image may be used for estimating VBD (**Paper IV**). If this is incorporated in the calculation, better assessments of the individual glandular dose could be obtained.

Paper V indicated that the individual glandular dose (per unit incident air kerma) could be estimated using the simulation procedure and breast phantoms recreated from BT volumes. Although the simulation procedure involves several approximations, the 3D localization of glandular tissue was probably the main source of the discrepancies in glandular dose estimates. The segmentation is a challenging task due to the limited depth resolution and small attenuation differences between adipose and glandular tissue, and it may be even more challenging for human cases than software phantoms. However, tissue segmentation of reconstructed BT volumes has been performed in some studies (Vedantham *et al.* 2011, Geeraert 2014), and the methods will most likely benefit from future development in image processing.

Future perspectives

In future breast cancer screening programmes, BT may be the primary examination method. The presented simulation procedure (**Paper I**) has been a useful tool in optimizing image acquisition parameters and estimating glandular dose. With progress in modelling software breast phantoms and lesions, VBD assessment, and segmentation methods, the procedure could be used in further evaluations of the BT imaging chain, and perhaps in estimating individual glandular dose for human cases. More precisely, it could be of interest to use the simulation procedure to investigate other acquisition schemes than the ones included in **Paper II** (e.g., with different numbers of projection images) and for soft tissue masses, as well as microcalcifications of different sizes. The long-term goal of the glandular dose simulations (**Paper V**) would be to develop and optimize the method for human cases and implement it in a possible BT screening programme.

6. Conclusions

In this thesis, a simulation procedure for use in the optimization of image acquisition and estimation of individual glandular dose in BT was developed.

The conclusions, in accordance with the specific aims of this thesis, are:

- The developed simulation procedure can be used to generate BT images with realistic sharpness if higher image noise and contrast compared to experimentally acquired images are acceptable (**Paper I**).
- For simulated microcalcifications, image acquisitions with very high central dose yielded significantly lower SDNR than acquisitions with more uniform dose distributions, and depth resolution increased with wider angular range. Accordingly, none of the evaluated acquisitions outperformed acquisition with an angular range of 50° and uniform projection and dose distribution (**Paper II**).
- It appears to be possible to approximately quantify and locate dense tissue within the breast using reconstructed BT volumes (**Paper III**).
- With prototype software, automatic and objective estimates of VBD could be obtained based on BT with similar performance as DM (**Paper IV**).
- Using software breast phantoms recreated from reconstructed BT volumes, the glandular dose could be estimated with good overall accuracy for breast phantoms with different glandularities and glandular distributions (**Paper V**).

Acknowledgements

occhiolism

n. *the awareness of the smallness of your perspective, by which you couldn't possibly draw any meaningful conclusions at all, about the world or the past or the complexities of culture, because although your life is an epic and unrepeatable anecdote, it still only has a sample size of one, and may end up being the control for a much wilder experiment happening in the next room.*

John Koenig, The Dictionary of Obscure Sorrows

I would like to express my sincere gratitude and appreciation to all of the people who have helped and supported me in the work of this thesis.

In particular, I would like to thank:

My supervisors

Anders Tingberg, Pontus Timberg, and Sophia Zackrisson – for giving me this opportunity, guidance and insightful advice, and for always being kind.

The LUCI research team

Daniel Förnvik (for being my everything), Magnus Dustler (for all the relevant and irrelevant everyday discussions), Hanna Sartor, Kristina Lång, Ingvar Andersson, Aldana Rosso, Kristin Johnson, Anna Hwasser, and Eva Prahl – a wonderful group of truly inspiring individuals.

My co-authors

Lucy Warren, for advice and practical assistance regarding the validation process.

Andreas Fieselmann, for advice and practical assistance in numerous collaborations.

International researchers in the field

Andreu Badal, for kind and patient guidance during the start-up and development of the simulation procedure.

Predrag Bakic, for generously sharing the software breast phantom and lots of ideas.

Anna Jerebko, Michael Kelm, Shiras Abdurahman, Julia Wicklein, Ludwig Ritschl, and Thomas Mertelmeier at Siemens – for long and rewarding collaboration.

Colleagues at Medical Radiation Physics, Malmö

Lars E. Olsson, Viveca Flodén, Sören Mattsson, Christopher Rääf, Martin Andersson, Lena Trinh, Lars Herrnsdorf, Simon Kindvall, Lovisa Waldner, Emma Olsson, Irma Mahmutovic Persson, Christian Bernhardsson, Marie Sydoff, Pernilla Peterson, Maria Christiansson, Jonas Nilsson, Ünal Ören, Therése Geber-Bergstrand, Karl Östlund, Marie-Louise Aurumskjöld, Mattias Jönsson, Kurt Sundin, Carl Siversson, Joana Boita, Antanas Bukartas, Guillaume Pedehontaa-Hiaa, Mikael Gunnarsson, Marcus Söderberg, Bea Jutemark Kvam, Peter Wallenius, Veronica Lindström, Olle Bruér, Sigrid Leide Svegborn, Sven Månsson, Anja Almén, Mikael Peterson, David Minarik, Erika Elgström, Renata Madru, Mats Nilsson, Christer Samuelsson, Jonas Jarneborn, Marcus Persson, Hanna Nicklasson, Mats Hansson, Jonas Svensson, Emelie Lind, Kai Nilsson, and Bengt Hemdal

My family and friends

Those closest to me – for everything you have done and will do for me.

Bibliography

Abdurahman, S., Jerebko, A., Mertelmeier, T., *et al.* 'Out-of-plane artifact reduction in tomosynthesis based on regression modeling and outlier detection'. *Breast Imaging, International Workshop on Digital Mammography 2012*, LNCS 7361, 729-736 (2012)

Abdurahman, S., Dennerlein, F., Jerebko, A., *et al.* 'Optimizing high resolution reconstruction in digital breast tomosynthesis using filtered back projection'. *Breast Imaging, International Workshop on Digital Mammography 2014*, LNCS 8539, 520-527 (2014)

Agostinelli, S., Allison, J., Amako, K. a., *et al.* 'GEANT4—a simulation toolkit'. *Nuclear Instruments and Methods in Physics Research Section A: Accelerators, Spectrometers, Detectors and Associated Equipment*, 506 (3), 250-303 (2003)

Allison, J., Amako, K., Apostolakis, J., *et al.* 'Geant4 developments and applications'. *IEEE Transactions on Nuclear Science*, 53 (1), 270-278 (2006)

Bakic, P. R., Zhang, C. and Maidment, A. D. 'Development and characterization of an anthropomorphic breast software phantom based upon region-growing algorithm'. *Medical Physics*, 38 (6Part1), 3165-3176 (2011)

Berger, M. and Seltzer, S. 'Response functions for sodium iodide scintillation detectors'. *Nuclear Instruments and Methods*, 104 (2), 317-332 (1972)

Berger, M. J. 'Monte Carlo calculation of the penetration and diffusion of fast charged particles'. In: Alder, B., Fernbach, S., Rotenberg, M. (eds.) Methods in Computational Physics, Volume 1, pp. 135-215. Academic Press, New Work (1963)

Boone, J. M. 'Spectral modeling and compilation of quantum fluence in radiography and mammography'. *Proceedings of SPIE, Medical Imaging 1998: Physics of Medical Imaging*, 3336, 592-602 (1998)

Boyd, N. F., Martin, L. J., Bronskill, M., *et al.* 'Breast tissue composition and susceptibility to breast cancer'. *Journal of the National Cancer Institute*, 102 (16), 1224-1237 (2010)

Boyd, N. F., Martin, L. J., Yaffe, M. J., *et al.* 'Mammographic density and breast cancer risk: current understanding and future prospects'. *Breast Cancer Research*, 13 (6), 223 (2011)

Byng, J. W., Boyd, N., Fishell, E., *et al.* 'The quantitative analysis of mammographic densities'. *Physics in Medicine & Biology*, 39 (10), 1629-1638 (1994)

Chan, H.-P. and Doi, K. 'The validity of Monte Carlo simulation in studies of scattered radiation in diagnostic radiology'. *Physics in Medicine & Biology*, 28 (2), 109-129 (1983)

Ciatto, S., Houssami, N., Apruzzese, A., *et al.* 'Categorizing breast mammographic density: intra-and interobserver reproducibility of BI-RADS density categories'. *The Breast*, 14 (4), 269-275 (2005)

Ciatto, S., Houssami, N., Bernardi, D., *et al.* 'Integration of 3D digital mammography with tomosynthesis for population breast-cancer screening (STORM): a prospective comparison study'. *The Lancet Oncology*, 14 (7), 583-589 (2013)

D'Orsi, C. J., Sickles, E. A., Mendelson, E. B., *et al.* 'ACR BI-RADS® Atlas, Breast Imaging Reporting and Data System'. American College of Radiology, Reston, VA (2013)

Dance, D. 'Monte-Carlo calculation of conversion factors for the estimation of mean glandular breast dose'. *Physics in Medicine & Biology*, 35 (9), 1211-1219 (1990)

Dance, D., Skinner, C., Young, K., *et al.* 'Additional factors for the estimation of mean glandular breast dose using the UK mammography dosimetry protocol'. *Physics in Medicine & Biology*, 45 (11), 3225-3240 (2000)

Dance, D., Hunt, R., Bakic, P., *et al.* 'Breast dosimetry using high-resolution voxel phantoms'. *Radiation Protection Dosimetry*, 114 (1-3), 359-363 (2005)

Dance, D., Young, K. and Van Engen, R. 'Further factors for the estimation of mean glandular dose using the United Kingdom, European and IAEA breast dosimetry protocols'. *Physics in Medicine & Biology*, 54 (14), 4361-4372 (2009)

Dance, D., Young, K. and Van Engen, R. 'Estimation of mean glandular dose for breast tomosynthesis: factors for use with the UK, European and IAEA breast dosimetry protocols'. *Physics in Medicine & Biology*, 56 (2), 453-471 (2010)

Dustler, M., Bakic, P., Petersson, H., *et al.* 'Application of the fractal Perlin noise algorithm for the generation of simulated breast tissue'. *Proceedings of SPIE, Medical Imaging 2015: Physics of Medical Imaging*, 9412, 94123E (2015)

Elangovan, P., Warren, L. M., Mackenzie, A., *et al.* 'Development and validation of a modelling framework for simulating 2D-mammography and breast tomosynthesis images'. *Physics in Medicine & Biology*, 59 (15), 4275-4293 (2014)

Evans, D. G. and Howell, A. 'Can the breast screening appointment be used to provide risk assessment and prevention advice?'. *Breast Cancer Research*, 17 (1), 84 (2015)

Fandos-Morera, A., Prats-Esteve, M., Tura-Soteras, J., *et al.* 'Breast tumors: composition of microcalcifications'. *Radiology*, 169 (2), 325-327 (1988)

Fieselmann, A., Jerebko, A. K. and Mertelmeier, T. 'Volumetric breast density combined with masking risk: enhanced characterization of breast density from mammography images'. *Breast Imaging, International Workshop on Digital Mammography 2016*, LNCS 9699, 486-492 (2016)

Fieselmann, A., Förnvik, D., Förnvik, H., *et al.* 'Volumetric breast density measurement for personalized screening: accuracy, reproducibility, and agreement with visual assessment'. *Submitted to International Workshop on Breast Imaging 2018* (2018)

Fitzgerald, M., Dance, D. R., Fisher, K., *et al.* 'Commissioning and Routine Testing of Mammographic X-Ray Systems'. Institute of Physical Sciences in Medicine, Report 59, England (1989)

Geeraert, N. 'Quantitative evaluation of fibroglandular tissue for estimation of tissue-differentiated absorbed energy in breast tomosynthesis'. Signal and Image processing, Télécom ParisTech (2014)

Geeraert, N., Klausz, R., Cockmartin, L.*, et al.* 'Comparison of volumetric breast density estimations from mammography and thorax CT'. *Physics in Medicine & Biology*, 59 (15), 4391-4409 (2014)

Geeraert, N., Klausz, R., Muller, S., *et al.* 'Evaluation of exposure in mammography: limitations of average glandular dose and proposal of a new quantity'. *Radiation Protection Dosimetry*, 165 (1-4), 342-345 (2015)

Giordano, L., Von Karsa, L., Tomatis, M., *et al.* 'Mammographic screening programmes in Europe: organization, coverage and participation'. *Journal of Medical Screening*, 19 (1_suppl), 72-82 (2012)

Gram, I. T., Funkhouser, E. and Tabár, L. 'The Tabar classification of mammographic parenchymal patterns'. *European Journal of Radiology*, 24 (2), 131-136 (1997)

Harris, S. 'An Introduction to the Theory of the Boltzmann Equation'. Holt, Rinehart & Winston, New York (1971) (Reprint, New York: Dover Publications, 2004)

Hartman, K., Highnam, R., Warren, R.*, et al.* 'Volumetric assessment of breast tissue composition from FFDM images'. *Digital Mammography, International Workshop on Digital Mammography 2008*, LNCS 5116, 33-39 (2008)

Hayward, E. and Hubbell, J. 'The albedo of various materials for 1-Mev photons'. *Physical Review*, 93 (5), 955-956 (1954)

Highnam, R., Brady, M., Yaffe, M. J.*, et al.* 'Robust breast composition measurement-VolparaTM'. *Digital Mammography, International Workshop on Digital Mammography 2010*, LNCS 6136, 342-349 (2010)

Howell, A., Anderson, A. S., Clarke, R. B.*, et al.* 'Risk determination and prevention of breast cancer'. *Breast Cancer Research*, 16 (5), 446 (2014)

Hubbell, J., Gimm, H. A. and Øverbø, I. 'Pair, triplet, and total atomic cross sections (and mass attenuation coefficients) for 1 MeV-100 GeV photons in elements Z=1 to 100'. *Journal of Physical and Chemical Reference Data*, 9 (4), 1023-1147 (1980)

Hubbell, J. 'Photon mass attenuation and energy-absorption coefficients'. *The International Journal of Applied Radiation and Isotopes*, 33 (11), 1269-1290 (1982)

IAEA. 'Dosimetry in Diagnostic Radiology: An International Code of Practice'. Technical Reports Series No. 457, International Atomic Energy Agency, Vienna (2007)

ICRP. 'The 2007 Recommendations of the International Commission on Radiological Protection'. ICRP Publication 103, Ann. ICRP 37 (2-4) (2007)

Jenkins, T. M., Nelson, W. R. and Rindi, A. (eds.) 'Monte Carlo Transport of Electrons and Photons'. Plenum Press, New York (1988)

Johns, P. C. and Yaffe, M. J. 'X-ray characterisation of normal and neoplastic breast tissues'. *Physics in Medicine & Biology*, 32 (6), 675-695 (1987)

Kawrakow, I. 'Accurate condensed history Monte Carlo simulation of electron transport. I. EGSnrc, the new EGS4 version'. *Medical Physics*, 27 (3), 485-498 (2000)

Laming, D. and Warren, R. 'Improving the detection of cancer in the screening of mammograms'. *Journal of Medical Screening*, 7 (1), 24-30 (2000)

Lauritsch, G. and Härer, W. H. 'Theoretical framework for filtered back projection in tomosynthesis'. *Proceedings of SPIE, Medical Imaging 1998: Image Processing*, 3338, 1127-1138 (1998)

Ljungberg, M. and Strand, S.-E. 'A Monte Carlo program for the simulation of scintillation camera characteristics'. *Computer Methods and Programs in Biomedicine*, 29 (4), 257-272 (1989)

Lång, K., Andersson, I., Rosso, A.*, et al.* 'Performance of one-view breast tomosynthesis as a stand-alone breast cancer screening modality: results from the Malmö Breast Tomosynthesis Screening Trial, a population-based study'. *European Radiology*, 26 (1), 184-190 (2016)

Machida, Y., Saita, A., Namba, H.*, et al.* 'Automated volumetric breast density estimation out of digital breast tomosynthesis data: feasibility study of a new software version'. *SpringerPlus*, 5 (1), 780 (2016)

Mertelmeier, T., Orman, J., Haerer, W.*, et al.* 'Optimizing filtered backprojection reconstruction for a breast tomosynthesis prototype device'. *Proceedings of SPIE, Medical Imaging 2006: Physics of Medical Imaging*, 6142, 61420F (2006)

Moore, A., Dance, D., Evans, D.*, et al.* 'The Commissioning and Routine Testing of Mammographic X-ray Systems'. Institute of Physics and Engineering in Medicine, Report 89, York (2005)

Olsson, Å., Sartor, H., Borgquist, S.*, et al.* 'Breast density and mode of detection in relation to breast cancer specific survival: a cohort study'. *BMC cancer*, 14 (1), 229 (2014)

Orman, J., Mertelmeier, T. and Haerer, W. 'Adaptation of image quality using various filter setups in the filtered backprojection approach for digital breast tomosynthesis'. *Digital Mammography, International Workshop on Digital Mammography 2006*, LNCS 4046, 175-182 (2006)

Pelowitz, D. B., Durkee, J. W., Elson, J. S.*, et al.* 'MCNPX 2.7 E Extensions'. LA-UR-11-01502, Los Alamos National Laboratory (2011)

Perry, N., Broeders, M., de Wolf, C.*, et al.* 'European guidelines for quality assurance in breast cancer screening and diagnosis. Fourth edition—summary document'. *Annals of Oncology*, 19 (4), 614-622 (2008)

Pertuz, S., McDonald, E. S., Weinstein, S. P.*, et al.* 'Fully automated quantitative estimation of volumetric breast density from digital breast tomosynthesis images: preliminary results and comparison with digital mammography and MR imaging'. *Radiology*, 279 (1), 65-74 (2015)

Poplack, S. P. 'Clinical applications of breast tomosynthesis'. In: Reiser, I., Glick, S. (eds.) *Tomosynthesis imaging*, pp. 181-187. Taylor & Francis, Boca Raton (2014)

Porras-Chaverri, M. A., Vetter, J. R. and Highnam, R. 'Personalizing mammographic dosimetry using multilayered anatomy-based breast models'. *Breast Imaging, International Workshop on Digital Mammography 2012*, LNCS 7361, 134-140 (2012)

Raeside, D. 'Monte Carlo principles and applications'. *Physics in Medicine & Biology*, 21 (2), 181-197 (1976)

Rogers, D., Faddegon, B., Ding, G.*, et al.* 'BEAM: a Monte Carlo code to simulate radiotherapy treatment units'. *Medical Physics*, 22 (5), 503-524 (1995)

Salvat, F., Fernández-Varea, J. M., Acosta, E.*, et al.* 'PENELOPE: A Code System for Monte Carlo Simulation of Electron and Photon Transport'. Proceedings of a Workshop/Training Course, NEA/NSC/DOC(2001)19, OECD/NEA (2001)

Sechopoulos, I., Bliznakova, K., Qin, X., *et al.* 'Characterization of the homogeneous tissue mixture approximation in breast imaging dosimetry'. *Medical Physics*, 39 (8), 5050-5059 (2012)

Sechopoulos[a], I. 'A review of breast tomosynthesis. Part I. The image acquisition process'. *Medical Physics*, 40 (1), 014301 (2013)

Sechopoulos[b], I. 'A review of breast tomosynthesis. Part II. Image reconstruction, processing and analysis, and advanced applications'. *Medical Physics*, 40 (1), 014302 (2013)

Seltzer, S. M. 'Calculation of photon mass energy-transfer and mass energy-absorption coefficients'. *Radiation Research*, 136 (2), 147-170 (1993)

Sempau, J., Acosta, E., Baro, J.*, et al.* 'An algorithm for Monte Carlo simulation of coupled electron-photon transport'. *Nuclear Instruments and Methods in Physics Research Section B: Beam Interactions with Materials and Atoms*, 132 (3), 377-390 (1997)

Sempau, J., Fernández-Varea, J., Acosta, E.*, et al.* 'Experimental benchmarks of the Monte Carlo code PENELOPE'. *Nuclear Instruments and Methods in Physics Research Section B: Beam Interactions with Materials and Atoms*, 207 (2), 107-123 (2003)

Sempau, J., Badal, A. and Brualla, L. 'A PENELOPE-based system for the automated Monte Carlo simulation of clinacs and voxelized geometries—application to far-from-axis fields'. *Medical Physics*, 38 (11), 5887-5895 (2011)

Shaheen, E., Van Ongeval, C., Zanca, F.*, et al.* 'The simulation of 3D microcalcification clusters in 2D digital mammography and breast tomosynthesis'. *Medical Physics*, 38 (12), 6659-6671 (2011)

Skaane, P., Bandos, A. I., Gullien, R.*, et al.* 'Comparison of digital mammography alone and digital mammography plus tomosynthesis in a population-based screening program'. *Radiology*, 267 (1), 47-56 (2013)

Smans, K., Zoetelief, J., Verbrugge, B.*, et al.* 'Simulation of image detectors in radiology for determination of scatter-to-primary ratios using Monte Carlo radiation transport code MCNP/MCNPX'. *Medical Physics*, 37 (5), 2082-2091 (2010)

Snyder, W., Cook, M., Nasset, E.*, et al.* 'Report of the Task Group on Reference Man'. ICRP Publication 23, International Commission on Radiological Protection (1975)

Socialstyrelsen. 'Cancer i siffror 2013 – Populärvetenskapliga fakta om cancer'. Artikelnr 2013-6-5, www.socialstyrelsen.se (2013)

Socialstyrelsen. 'Screening för bröstcancer - Rekommendation och bedömningsunderlag'. Artikelnr 2014-2-32, www.socialstyrelsen.se (2014)

Socialstyrelsen. 'Nationella riktlinjer för bröst-, prostata-, tjocktarms- och ändtarmscancervård'. Artikelnr 2014-4-2, www.socialstyrelsen.se (2015)

Socialstyrelsen. 'Statistikdatabas för cancer'. http://www.socialstyrelsen.se/statistik/statistikdatabas/cancer (accessed 3 April 2018)

Svalkvist, A. and Båth, M. 'Simulation of dose reduction in tomosynthesis'. *Medical Physics*, 37 (1), 258-269 (2010)

Tingberg, A. and Zackrisson, S. 'Digital mammography and tomosynthesis for breast cancer diagnosis'. *Expert Opinion on Medical Diagnostics*, 5 (6), 517-526 (2011)

van Engeland, S., Snoeren, P. R., Huisman, H.*, et al.* 'Volumetric breast density estimation from full-field digital mammograms'. *IEEE Transactions on Medical Imaging*, 25 (3), 273-282 (2006)

Warren, L., Green, F., Shrestha, L.*, et al.* 'Validation of simulation of calcifications for observer studies in digital mammography'. *Physics in Medicine & Biology*, 58 (16), N217–N228 (2013)

Vedantham, S., Shi, L., Karellas, A.*, et al.* 'Semi-automated segmentation and classification of digital breast tomosynthesis reconstructed images'. *Engineering in Medicine and Biology Society, 2011 Annual International Conference of the IEEE*, 6188-6191 (2011)

Wolfe[a], J. N. 'Breast patterns as an index of risk for developing breast cancer'. *American Journal of Roentgenology*, 126 (6), 1130-1137 (1976)

Wolfe[b], J. N. 'Risk for breast cancer development determined by mammographic parenchymal pattern'. *Cancer*, 37 (5), 2486-2492 (1976)

Woodard, H. and White, D. 'The composition of body tissues'. *The British Journal of Radiology*, 59 (708), 1209-1218 (1986)

Yaffe, M. J. 'Mammographic density. Measurement of mammographic density'. *Breast Cancer Research*, 10 (3), 209 (2008)

Zankl, M., Fill, U., Hoeschen, C., *et al.* 'Average glandular dose conversion coefficients for segmented breast voxel models'. *Radiation Protection Dosimetry*, 114 (1-3), 410-414 (2005)

Zeng, R., Park, S., Bakic, P., *et al.* 'Evaluating the sensitivity of the optimization of acquisition geometry to the choice of reconstruction algorithm in digital breast tomosynthesis through a simulation study'. *Physics in Medicine & Biology*, 60 (3), 1259-1288 (2015)

Zeng, R., Badano, A. and Myers, K. J. 'Optimization of digital breast tomosynthesis (DBT) acquisition parameters for human observers: effect of reconstruction algorithms'. *Physics in Medicine & Biology*, 62 (7), 2598-2611 (2017)

Zerby, C. D. 'A Monte Carlo calculation of the response of gamma-ray scintillation counters'. In: Alder, B., Fernbach, S., Rotenberg, M. (eds.) *Methods in Computational Physics, Volume 1*, pp. 89-134. Academic Press, New York (1963)

Zoetelief, J., Fitzgerald, M., Leitz, W.*, et al.* 'European Protocol on Dosimetry in Mammography'. EUR 16263 EN, European Commission (1996)

Oh, brilliant!

Jodie Whittaker as the Thirteenth Doctor

Printed by Media-Tryck, Lund 2018 NORDIC SWAN ECOLABEL 3041 0903

LUND UNIVERSITY

FACULTY OF MEDICINE

Medical Radiation Physics, Malmö

Lund University, Faculty of Medicine
Doctoral Dissertation Series 2018:71
ISBN 978-91-7619-637-3
ISSN 1652-8220